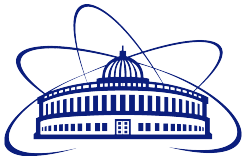

JOINT INSTITUTE FOR NUCLEAR RESEARCH
Veksler and Baldin laboratory of High Energy Physics

FINAL REPORT ON THE
SUMMER STUDENT PROGRAM

Performance study of directed and elliptic flow in the MPD experiment at NICA

Supervisor:
Dr. Vadim Ivanovich Kolesnikov

Scientific advisors:
Dr. Ilya Vladimirovich Selyuzhenkov, Germany
GSI, Darmstadt
Dr. Arkady Vladimirovich Taranenko, Russia
National Research Nuclear University MEPhI

Student:
Petr Parfenov, Russia
National Research Nuclear University MEPhI

Participation period:
July 16 – August 31

Dubna, 2018

Contents

Abstract

The main goal of the future MPD experiment at NICA is to explore the QCD phase diagram in the region of highly compressed and hot baryonic matter in the energy range corresponding to the highest chemical potential. Properties of such dense matter can be studied using azimuthal anisotropy which is categorized by the Fourier coefficients of the azimuthal distribution decomposition. Performance of the detector response based on simulations with realistic reconstruction procedure is presented for centrality determination, reaction plane estimation, directed and elliptic flow coefficients.

1 Introduction

1.1 Azimuthal flow

Studies of the quark-gluon matter thermodynamical properties is one of the main priorities in the number of experiments specializing in the heavy-ion physics [1]. Transverse azimuthally anisotropic flow measurements are one of the key methods to study the time evolution of the strongly interacted medium formed in the nucleous collisions. In the non-central collisions, initial spatial anisotropy results in the azimuthally anisotropic particle emission. The magnitude of the anisotropic flow is defined using the the Fourier coefficients $v_k\{\Psi_n\}$ of azimuthal distribution of the emitted particles with respect to the reaction plane [2]:

$$\frac{dN}{d(\varphi-\Psi_n)} = 1+2\sum_{k=1}^{\infty} v_k \cos\left[k(\varphi-\Psi_{RP})\right], \tag{1}$$

where φ – is the azimuthal angle of particle, k – is the harmonic order and Ψ_{RP} is the reaction plane angle. v_1 is hence called directed flow, v_2 – elliptic flow.

The finite number of fragments and the fluctuation of the charged particle multiplicity from one collision to another at fixed impact parameter orientation result in a difference between the experimentally measurable event plane and the reaction plane orientation. This difference is usually quantified in terms of the event plane resolution (a Gaussian width of the $(\Psi_{RP}-\Psi_{n,EP})$ distribution):

$$R_{n,EP} = \langle \cos\left[n(\Psi_{RP}-\Psi_{m,EP})\right]\rangle. \tag{2}$$

Resulting Fourier coefficients v_n are obtained as follows:

$$v_n = \frac{\langle \cos\left[n(\varphi-\Psi_{m,EP})\right]\rangle}{R_{n,EP}}. \tag{3}$$

In this analysis, first harmonic of the event plane $\Psi^{FHCal}_{1,EP}$, obtained via the energy deposition in the FHCal modules [3, 4], will be used.

1.2 Simulation setup

The used data (Au-Au, $\sqrt{s_{\rm NN}} = 11$ GeV) was generated via the UrQMD and LA-QGSM models [5, 6], GEANT (versions 3 and 4 – see details in the text below) and reconstructed using Cluster Finder tracking for the MPD experiment [7]. MPDROOT framework was used [8]. Original DSTfiles were converted into the lightweight PicoDst format which is fully compatible with the standard ROOT [9].

The simulated MPD geometry includes all detectors subsystems, among those are two parts of FHCal on left and right sides from the center of the MPD at the distance $3195\times 2 = 6390$ mm. Both parts of FHCal consists of 45 individual modules with the transverse module size being 15×15 cm^2. The central module has a hole for a beam pipe with the diameter 10 cm. Each module includes 42 lead/scintillator sandwiches with the total interaction length of about $4\lambda_i$. Every 6 consecutive layers of scintillators have individual readout, which provides the longitudinal segmentation of FHCal modules. To evaluate the effect of the MPD solenoidal magnet, the simulated axial magnetic field of 0.5 T is uniformly distributed between the FHCal parts.

2 Methods

2.1 Track selection

The following cuts were used for the further analysis (see Fig. 1):

- Transverse momentum cut: $0 < p_T \leq 3$ GeV/c
- Pseudorapidity cut: $|\eta| < 1.5$
- Cut on number of hits of the track in TPC: $N_{\text{hits}} > 32$
- Primary particles: 2σ DCA cut

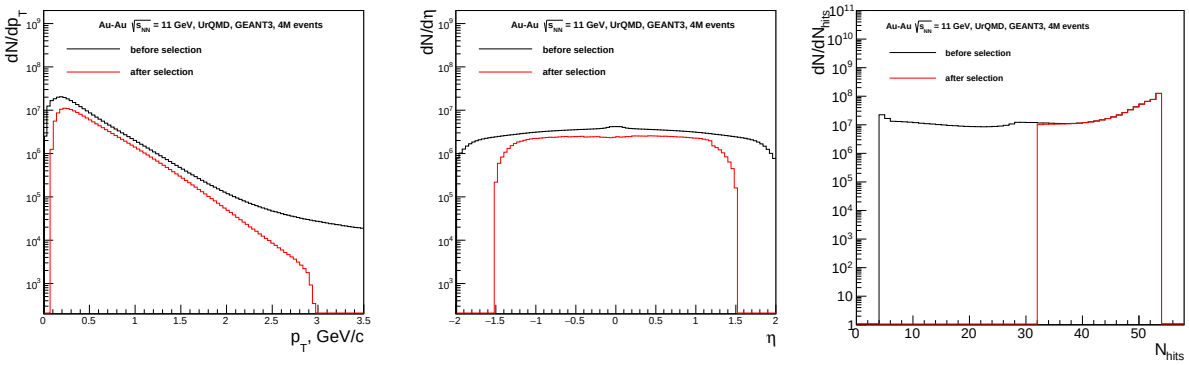

Fig. 1: (left) p_T (middle) η (right) N_{hits} distribution before and after track selection.

Fig. 2, 3 show resulting p_T and η distributions for different species (positively charged only) with the corresponding efficiency. Particles were identified via the PDG codes given from GEANT simulated data. Where the efficiency is defined as follows:

$$\begin{aligned} \text{Efficiency}^{p_T} &= \frac{\frac{dN}{dp_T}(\text{reco})}{\frac{dN}{dp_T}(\text{true})} \\ \text{Efficiency}^{\eta} &= \frac{\frac{dN}{d\eta}(\text{reco})}{\frac{dN}{d\eta}(\text{true})}. \end{aligned} \tag{4}$$

Based on pT efficiency distribution (see Fig. 2, bottom right), following p_T range was selected:

$$p_T > 0.2 \text{ GeV/c}. \tag{5}$$

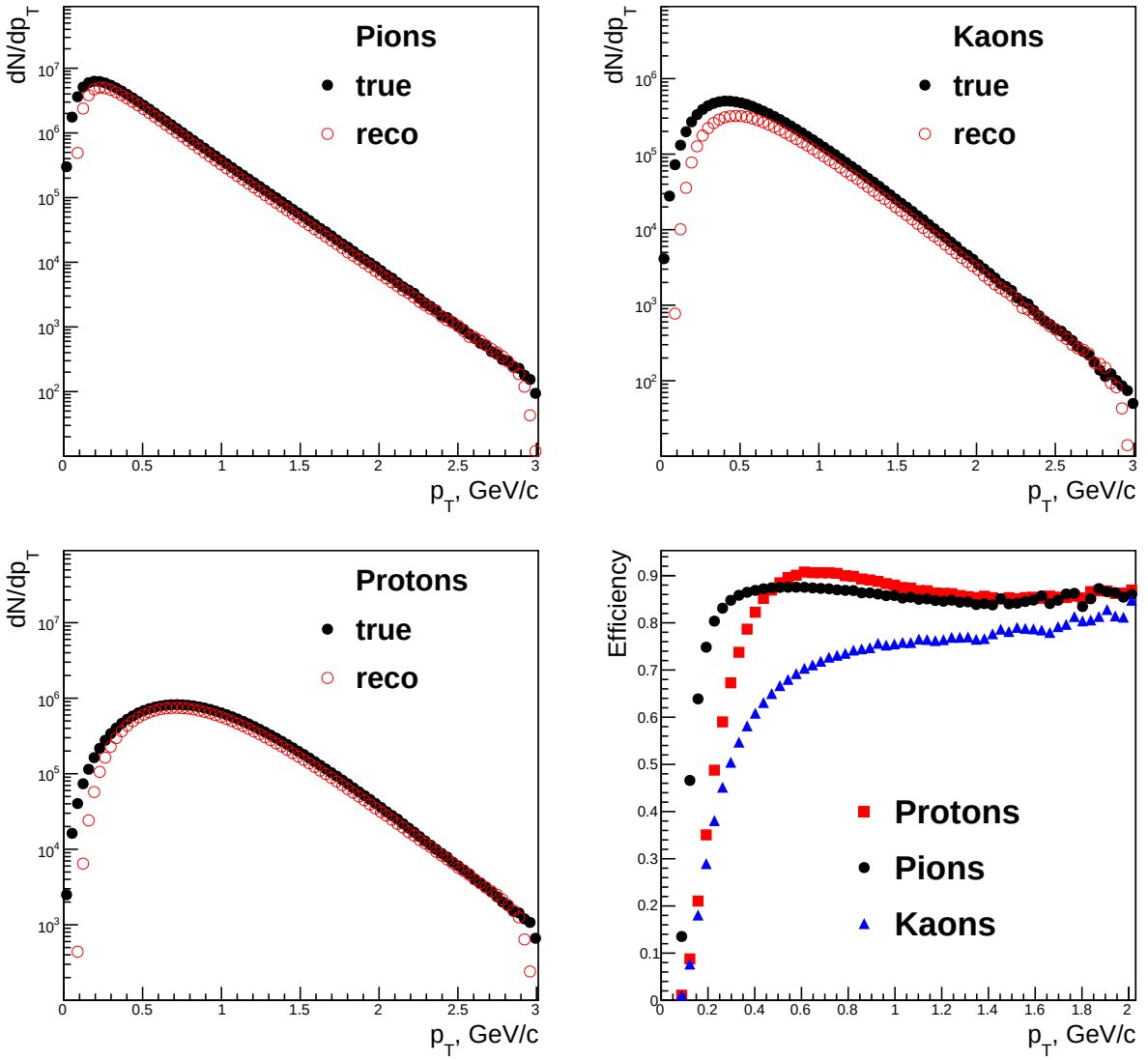

Fig. 2: p_T spectra of pion (upper left), kaons (upper right), protons (bottom left) and efficiency (bottom-right) of the tracks after selection. Particles were identified via PDG codes from GEANT.

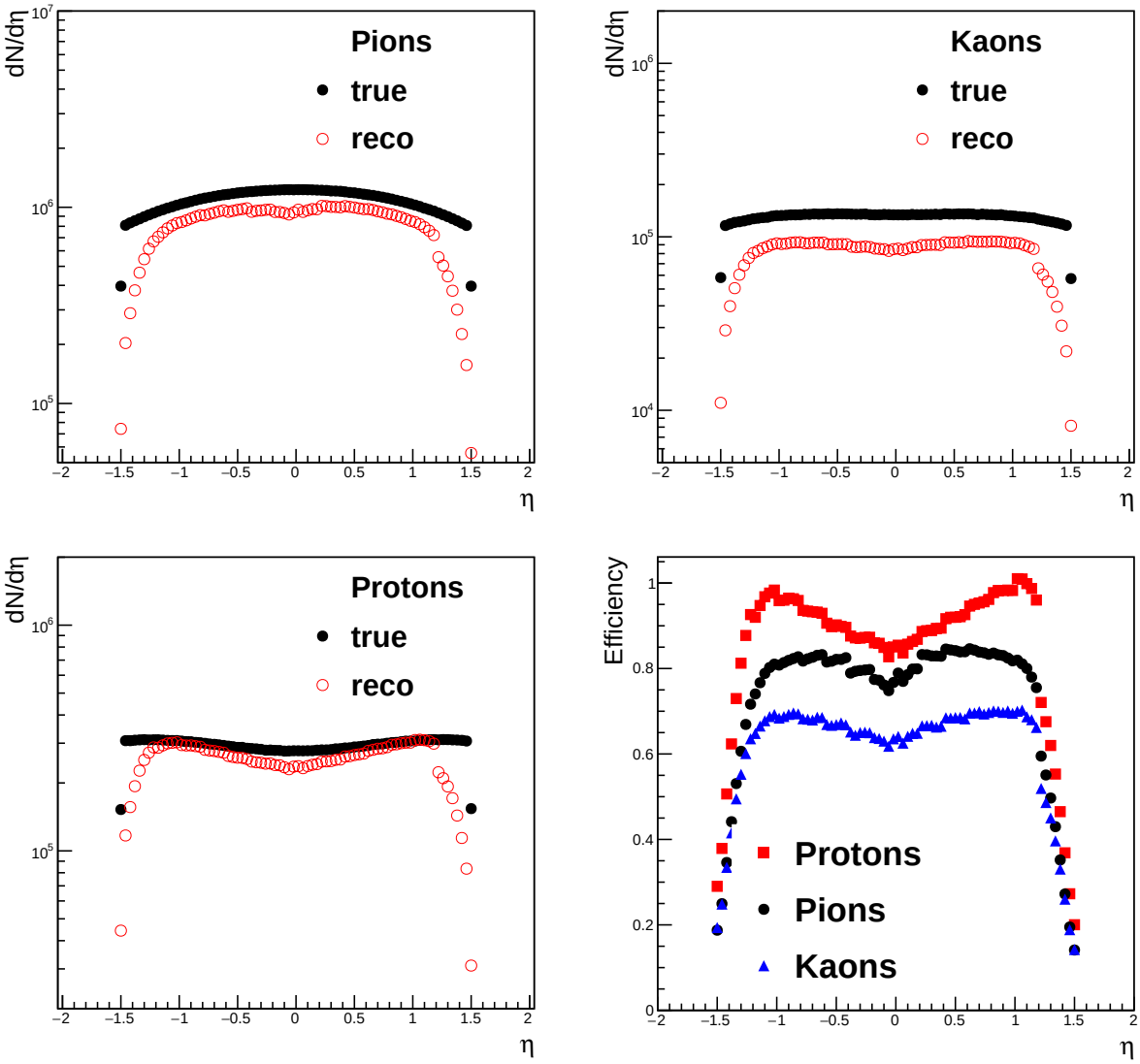

Fig. 3: η spectra of pion (upper left), kaons (upper right), protons (bottom left) and efficiency (bottom right) of the tracks after selection. Particles were identified via PDG codes from GEANT.

2.2 Centrality determination

Centrality was calculated based on the multiplicity of charged particles in TPC. Only primary tracks were taken into account. Resulting centrality resolution shown in the Fig. 4 denotes the normalized width of the impact parameter b distribution in the centrality bin. Centrality can be determined using multiplicity of the charged particles from TPC with the resolution 5-10% for the wide centrality range.

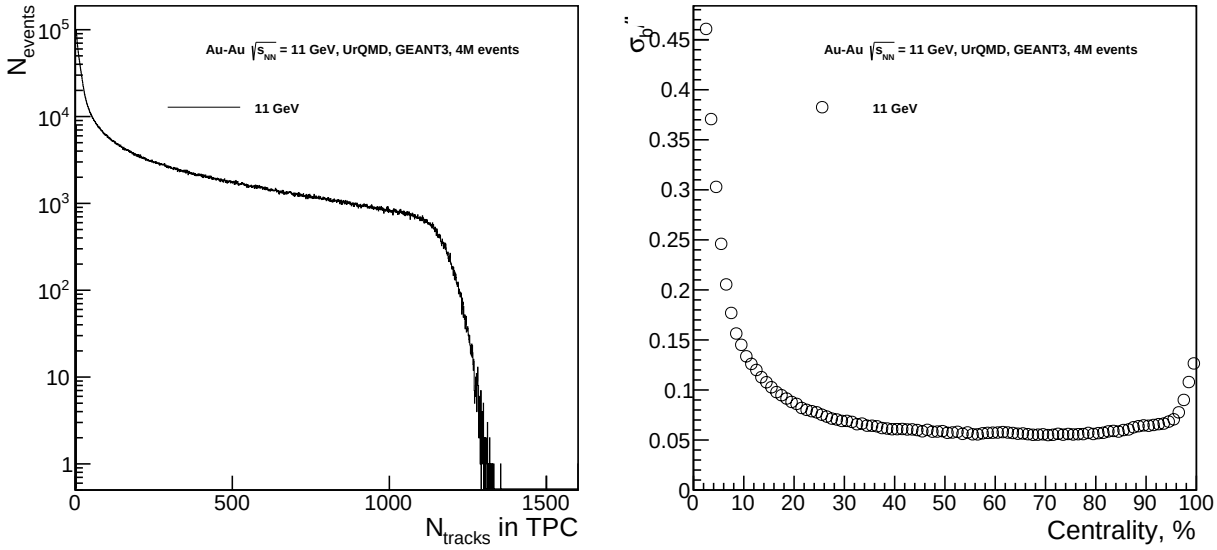

Fig. 4: (left) multiplicity of the charged particles in TPC, (right) centrality resolution.

2.3 Particle identification with TPC and TOF detectors

Realistic PID was done using combined method (TPC+TOF and TPC alone) which implemented in the MpdPid class in mpdroot framework [10]. MpdPid uses TPC alone method when the track lies in the outlier region on the m^2 vs p correlation plot (see Fig. 7). Used region of the total momentum $0 < p < 3$ GeV/c. In this analysis, only TPC tracks with matched TOF hits were selected. The fraction of the tracks with TOF hit compared to the all tracks is shown in the Fig. 5.

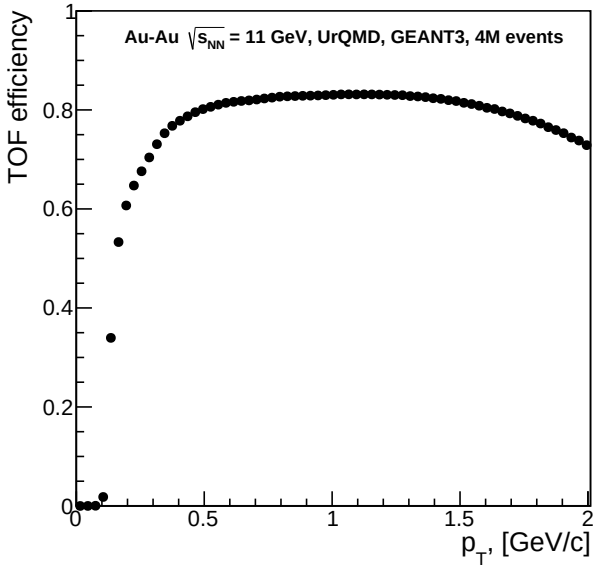

Fig. 5: p_T efficiency of the tracks with TOF hit.

Only positively charged particles are discussed in this analysis (see Fig. 6). Resulting m^2 as a function of momentum is shown in Fig. 7. The m^2 distributions for pions, kaons and protons are shown in Fig. 8, 9, 10.

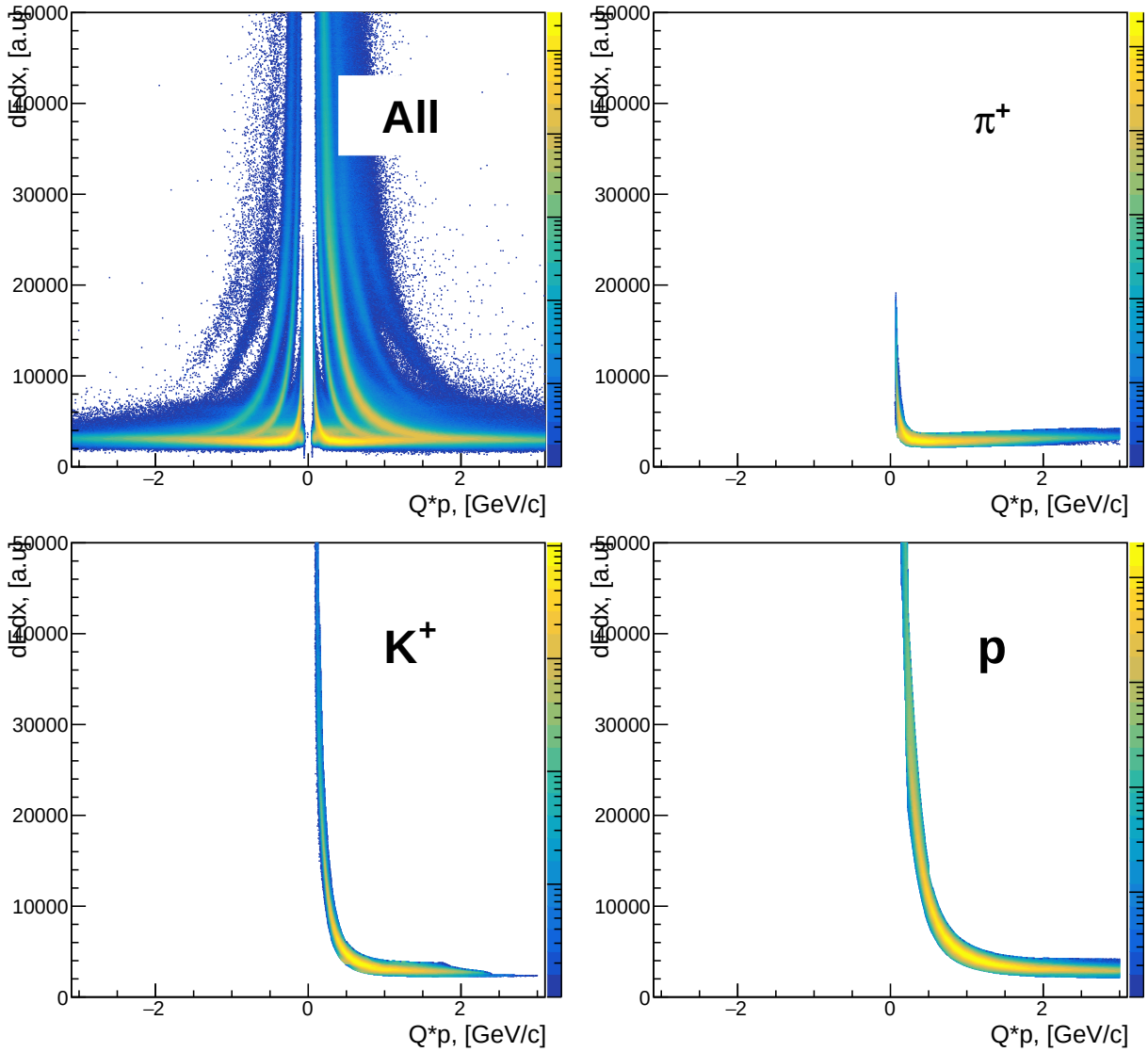

Fig. 6: dEdx vs Qp for all (upper left), pions (upper right), kaons (bottom left) and protons (bottom right) of the tracks after selection.

MpdPid results the probability of the track to be the certain particle specie. In this analysis, track is considered as a certain particle if the corresponding probability $P_{\text{particle}} > 90\%$.

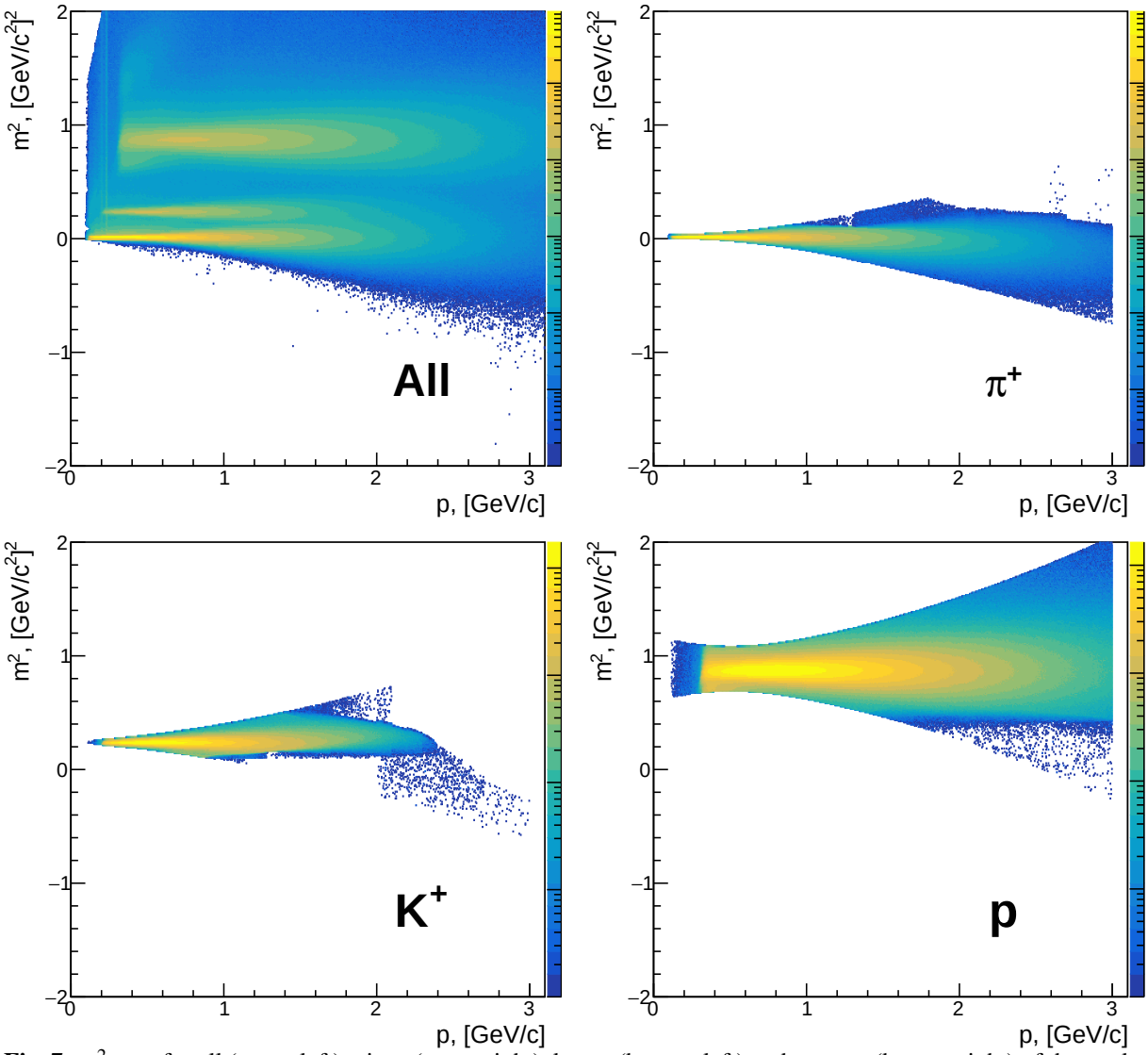

Fig. 7: m^2 vs p for all (upper left), pions (upper right), kaons (bottom left) and protons (bottom right) of the tracks after selection.

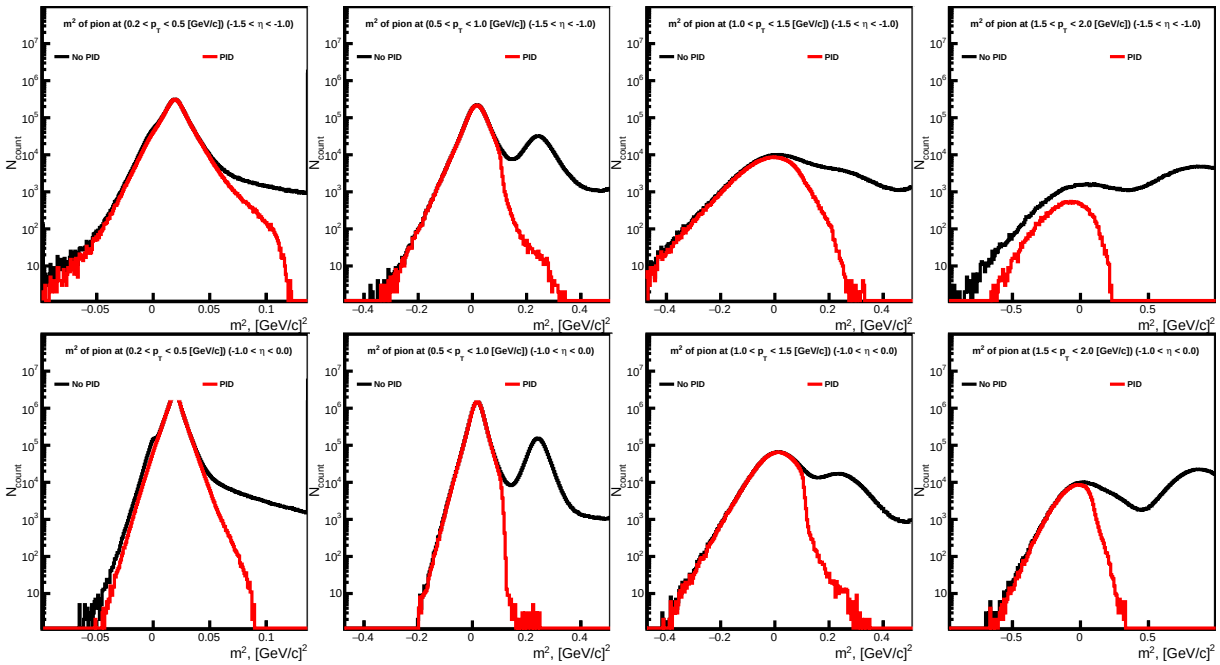

Fig. 8: m^2 distributions of the positively charged particles before (black line) and after (red line) PID cuts for pions.

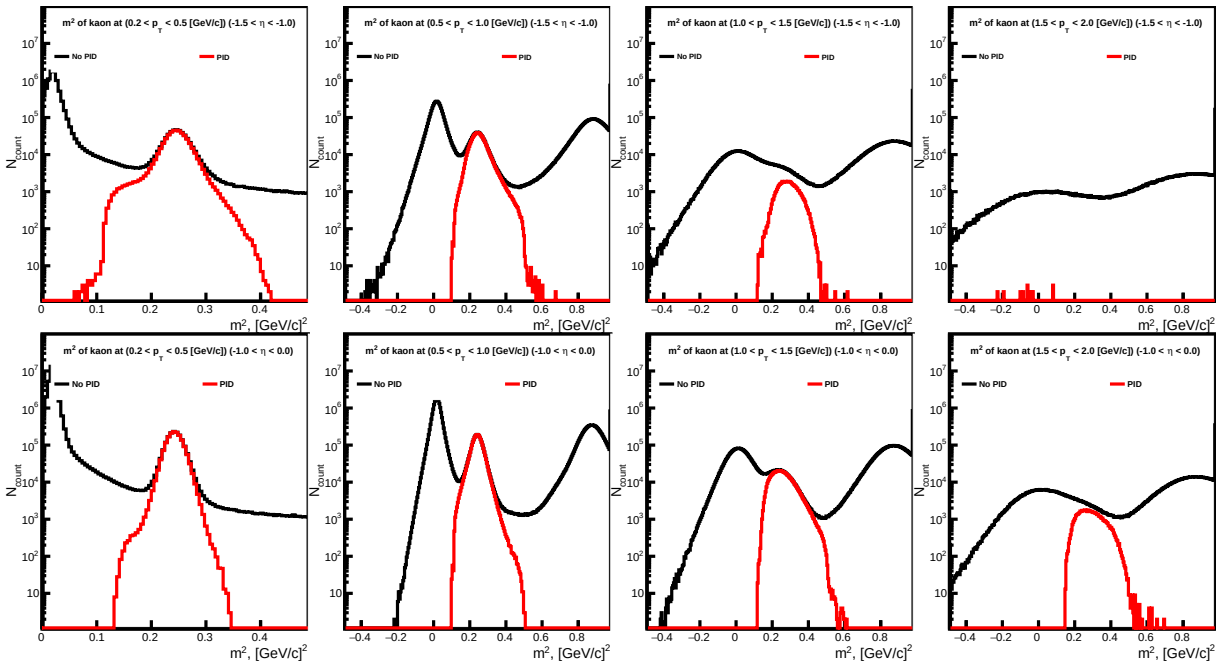

Fig. 9: m^2 distributions of the positively charged particles before (black line) and after (red line) PID cuts for kaons.

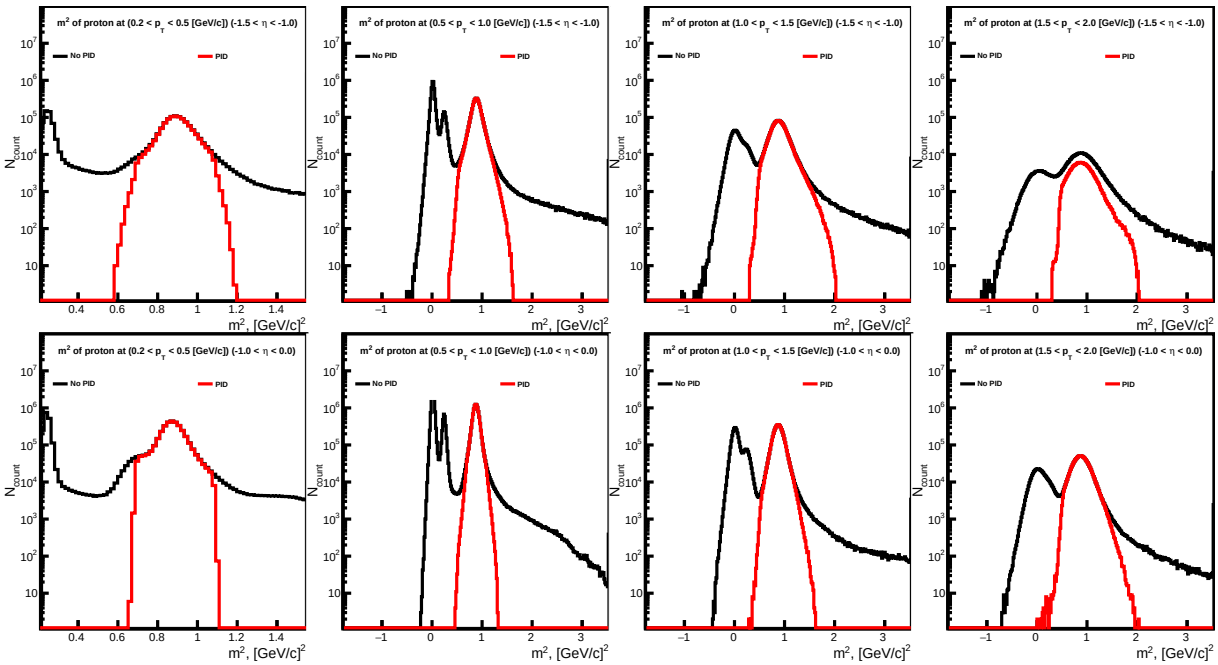

Fig. 10: m^2 distributions of the positively charged particles before (black line) and after (red line) PID cuts for protons.

3 Results

3.1 Event plane resolution

Event plane was calculated using the energy deposition in FHCal calorimeter modules (see Fig. 11).

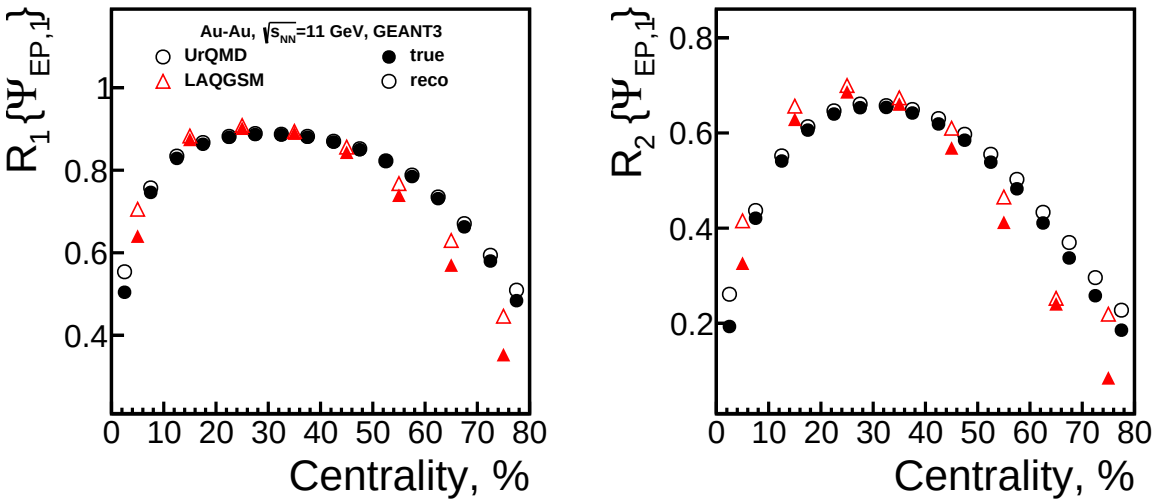

Fig. 11: Resolution correction factor for directed (left) and elliptic (right) flow. "true"("reco") denotes the result obtained for the reaction (FHCal event) plane.

3.1.1 GEANT3 vs GEANT4 comparison

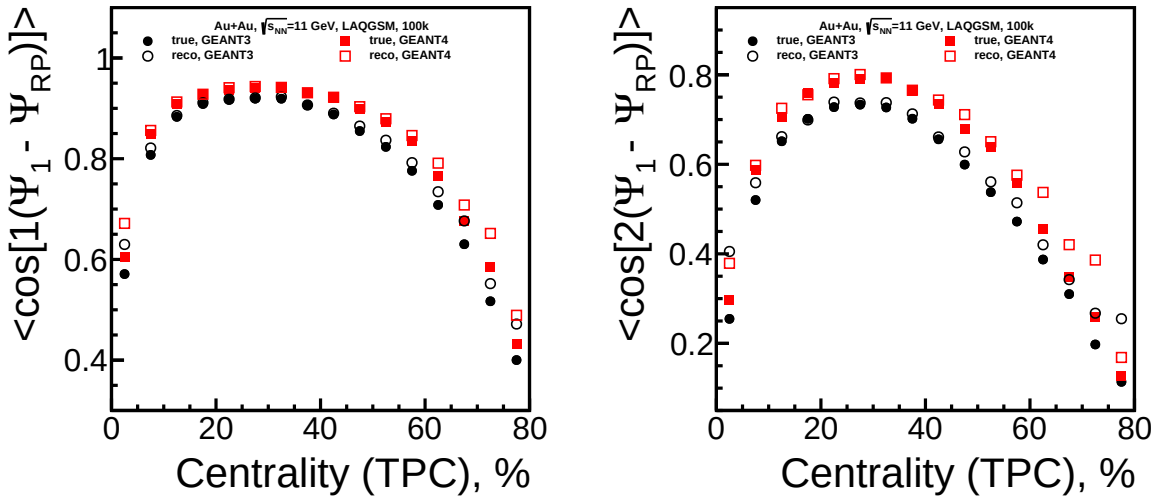

Fig. 12: Resolution correction factor for directed (left) and elliptic (right) flow. "true"("reco") denotes the result obtained for the reaction (FHCal event) plane using GEANT3 (circles) and GEANT4 (squares) frameworks.

3.2 Directed and elliptic flow as a function of p_T and y

Generated values for directed (v_1) and elliptic (v_2) flow on the plots below were taken alongside the reconstructed ones. Both generated and reconstructed values are shown as a function of the reconstructed p_T and y. Ideal PID (PDG codes from GEANT) that was used in the earlier analysis [11, 12] is compared to the realistic PID (MpdPid).

3.2.1 *Directed flow*

As for the p_T dependence of the directed flow, additional cut on rapidity $0.2 < |y| < 1.5$, and the symmetrization over y were made.

3.2.1.1 *Protons*

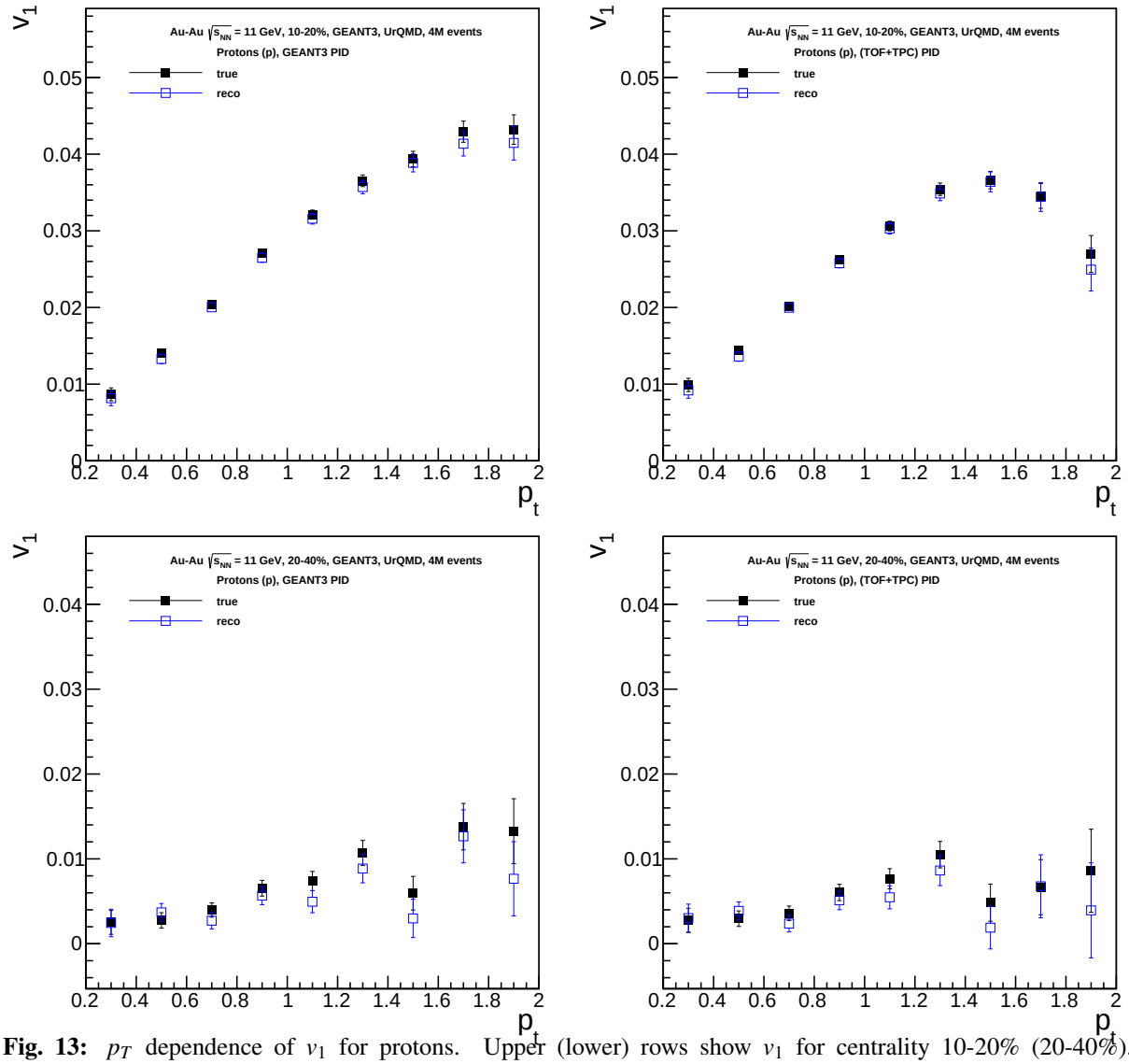

Fig. 13: p_T dependence of v_1 for protons. Upper (lower) rows show v_1 for centrality 10-20% (20-40%). Left (right) columns show ideal (realistic) PID. "true" ("reco") denotes the result obtained with generated from GEANT(reconstructed) values.

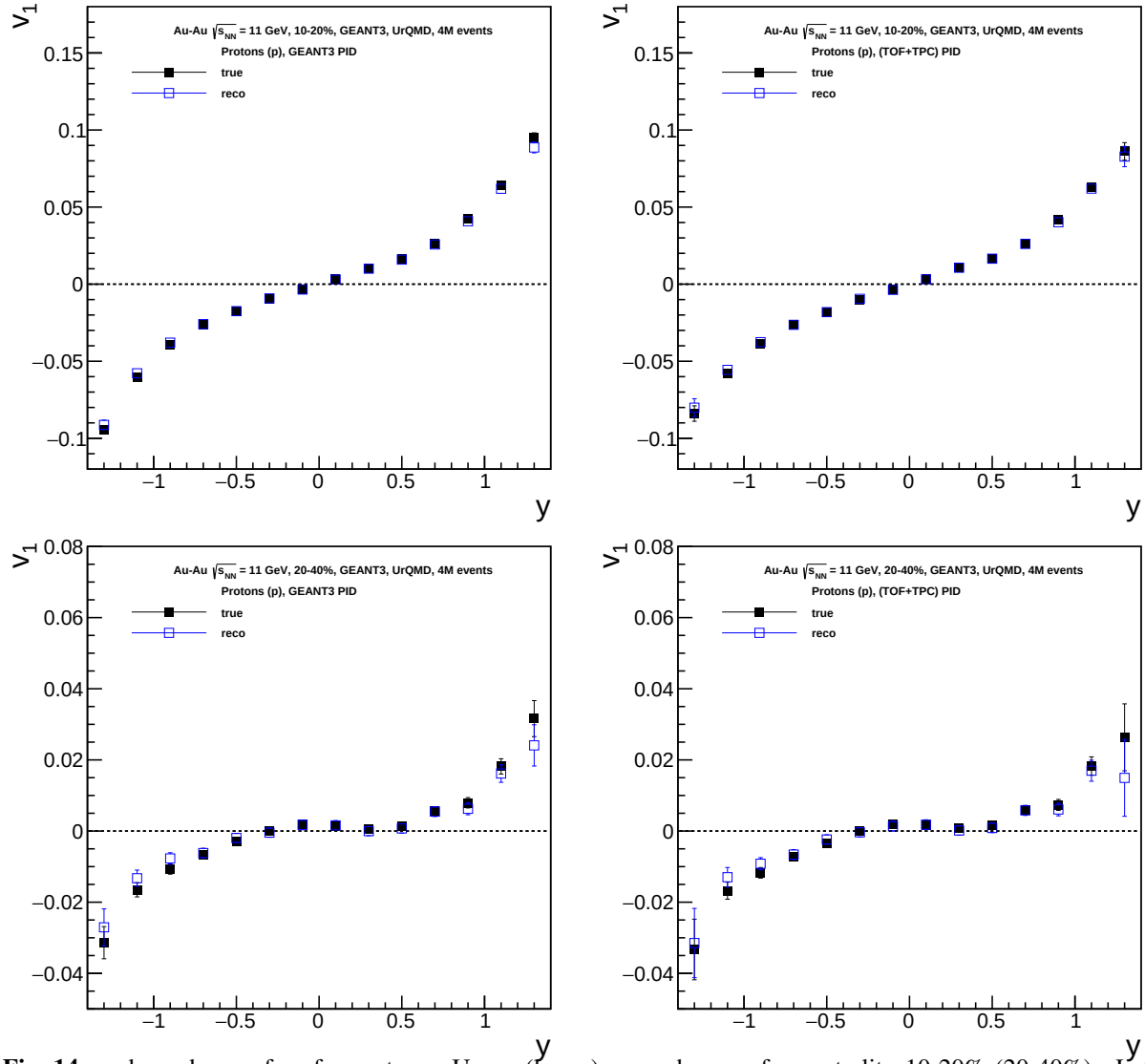

Fig. 14: y dependence of v_1 for protons. Upper (lower) rows show v_1 for centrality 10-20% (20-40%). Left (right) columns show ideal (realistic) PID. ”true” (”reco”) denotes the result obtained with generated from GEANT(reconstructed) values.

3.2.1.2 ***Kaons***

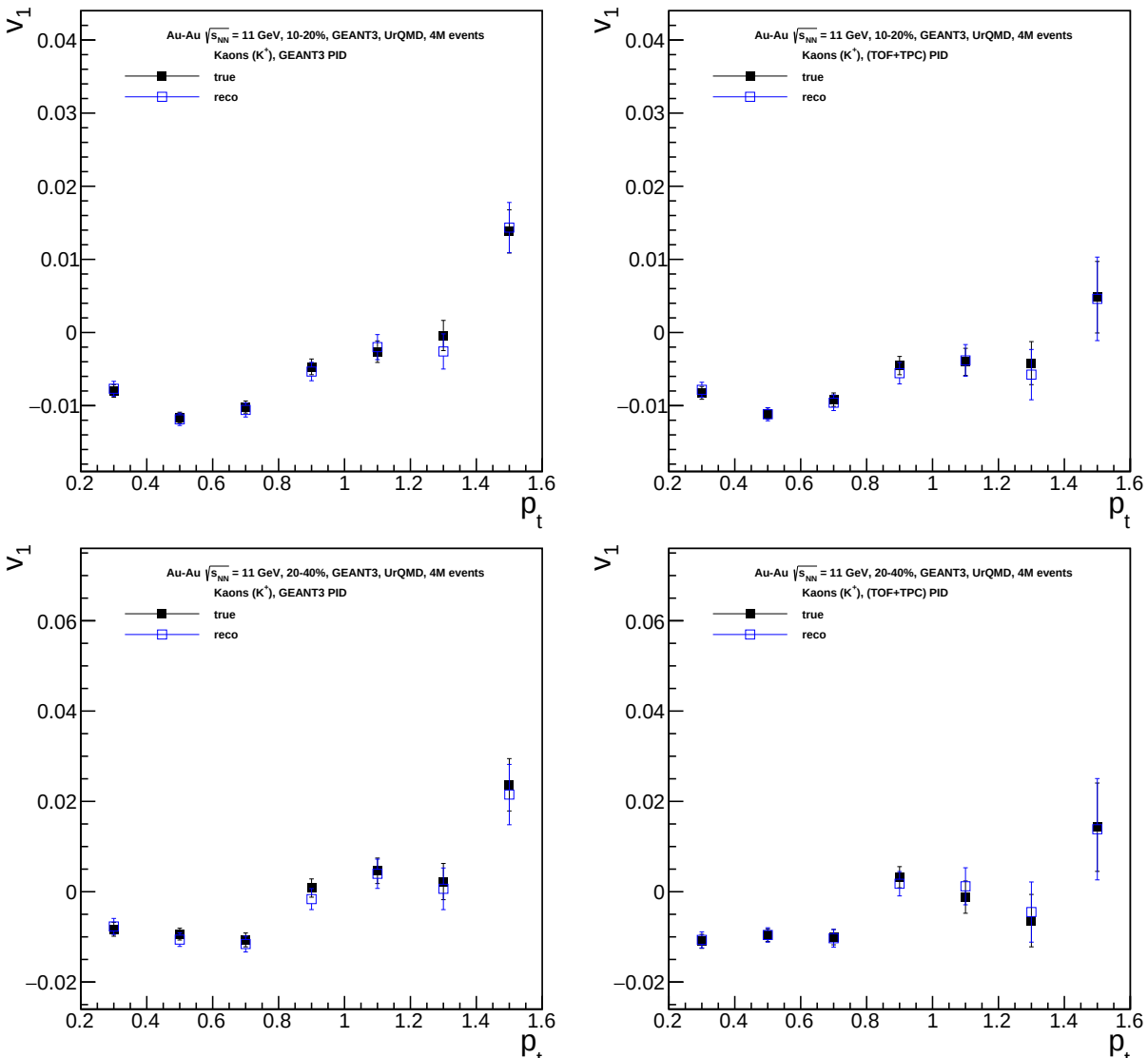

Fig. 15: p_T dependence of v_1 for kaons. Upper (lower) rows show v_1 for centrality 10-20% (20-40%). Left (right) columns show ideal (realistic) PID. "true" ("reco") denotes the result obtained with generated from GEANT(reconstructed) values.

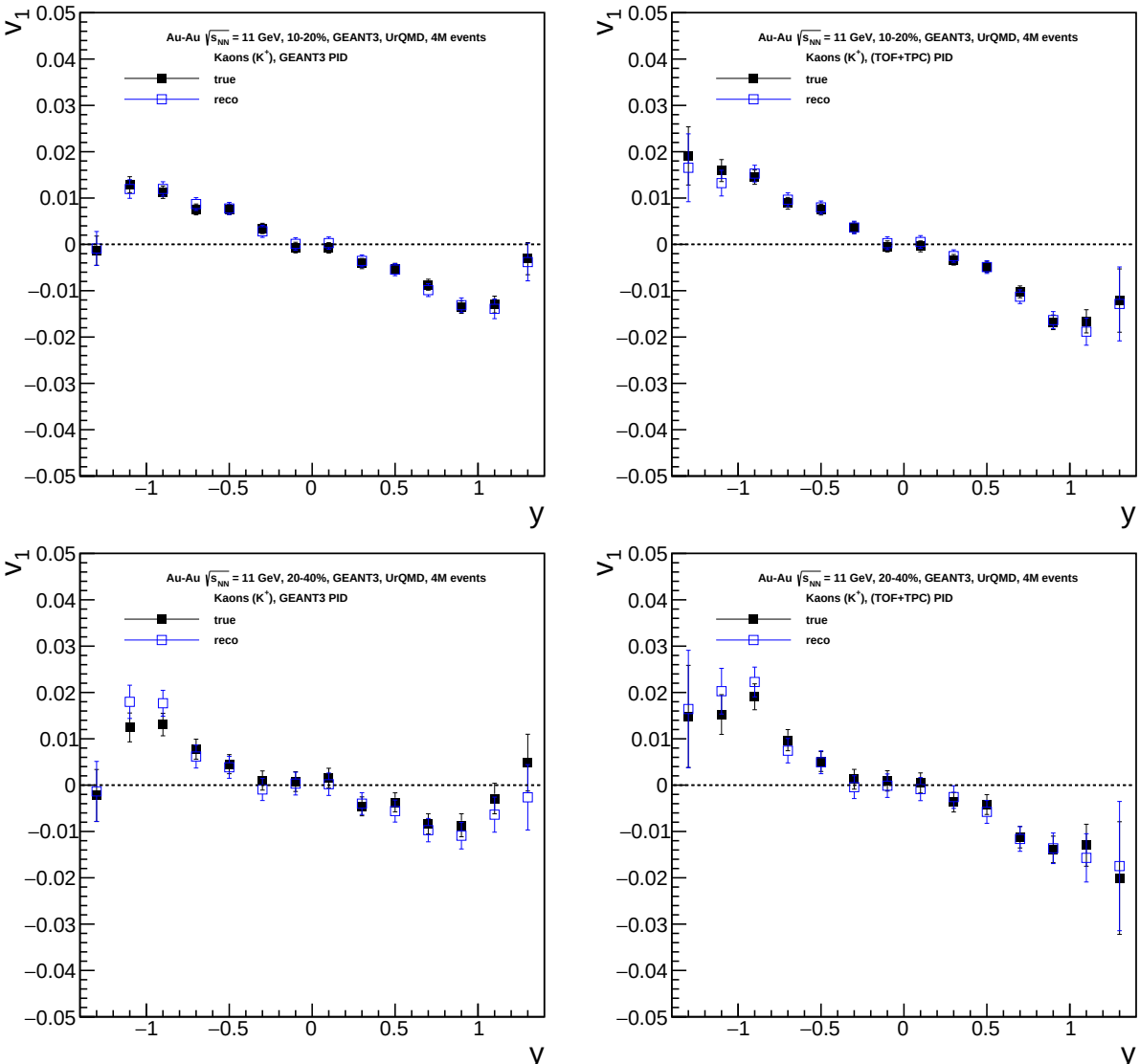

Fig. 16: y dependence of v_1 for kaons. Upper (lower) rows show v_1 for centrality 10-20% (20-40%). Left (right) columns show ideal (realistic) PID. ”true” (”reco”) denotes the result obtained with generated from GEANT(reconstructed) values.

3.2.1.3 *Pions*

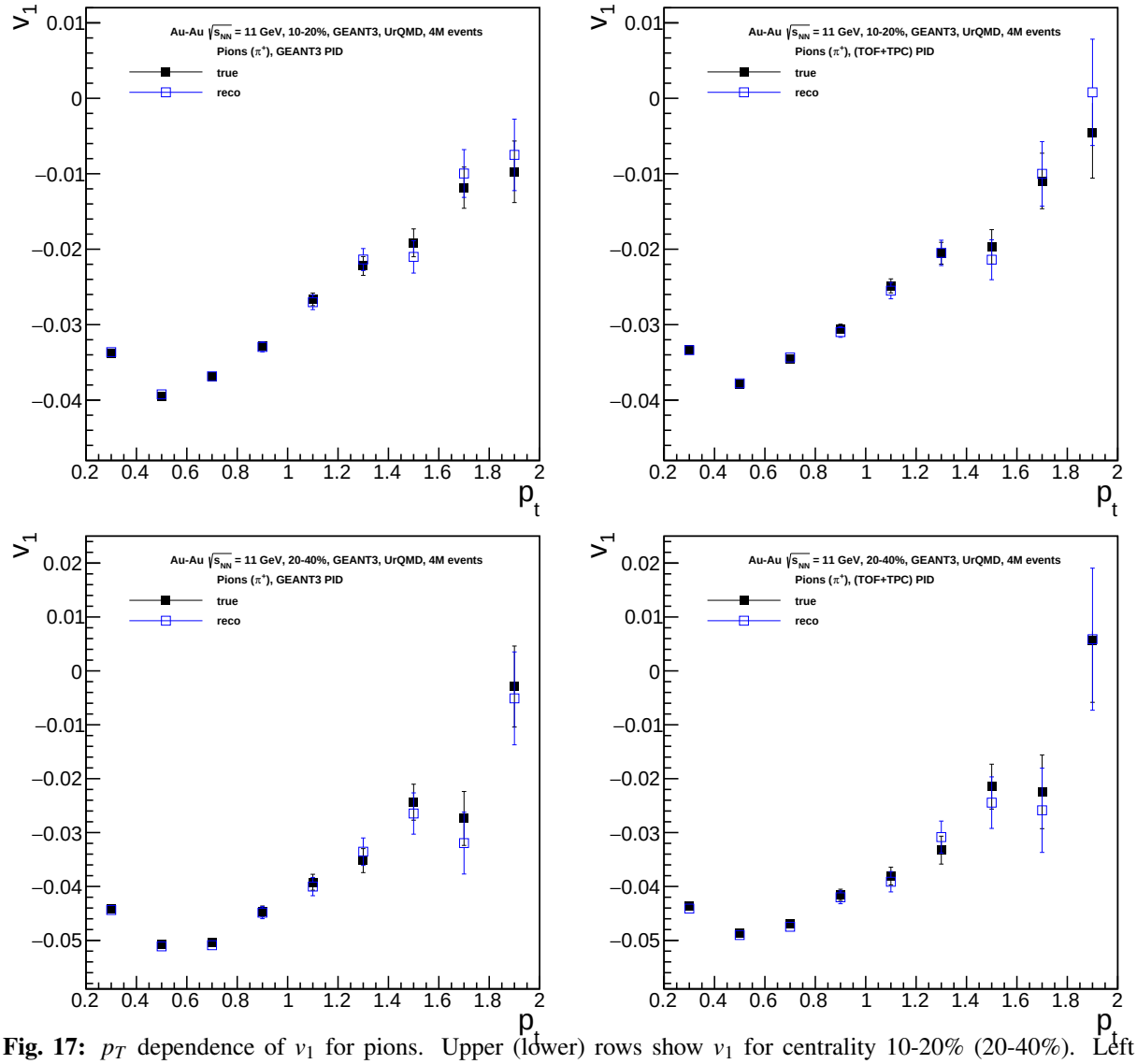

Fig. 17: p_T dependence of v_1 for pions. Upper (lower) rows show v_1 for centrality 10-20% (20-40%). Left (right) columns show ideal (realistic) PID. "true" ("reco") denotes the result obtained with generated from GEANT(reconstructed) values.

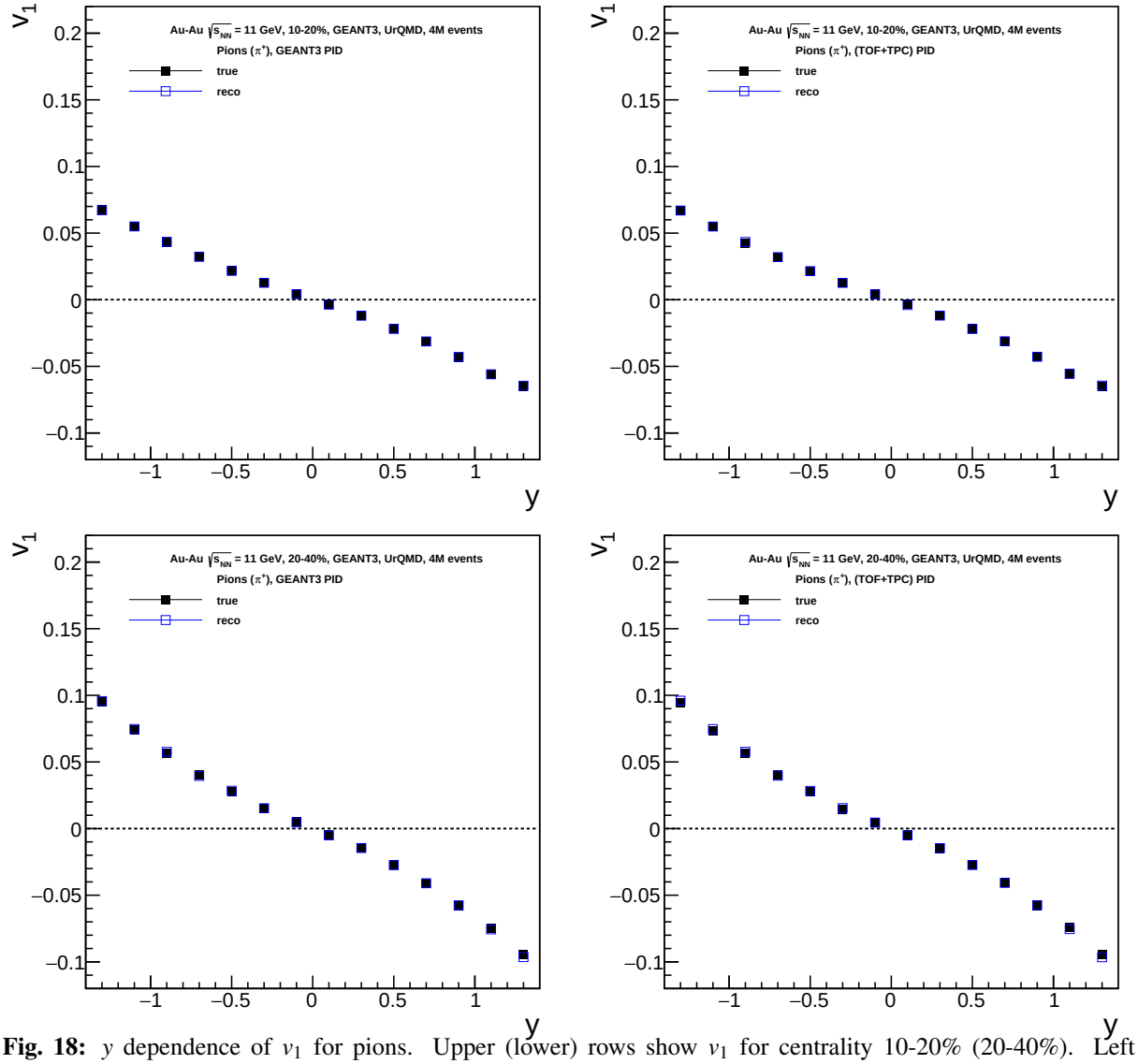

Fig. 18: y dependence of v_1 for pions. Upper (lower) rows show v_1 for centrality 10-20% (20-40%). Left (right) columns show ideal (realistic) PID. ”true” (”reco”) denotes the result obtained with generated from GEANT(reconstructed) values.

3.2.2 Elliptic flow

3.2.2.1 Protons

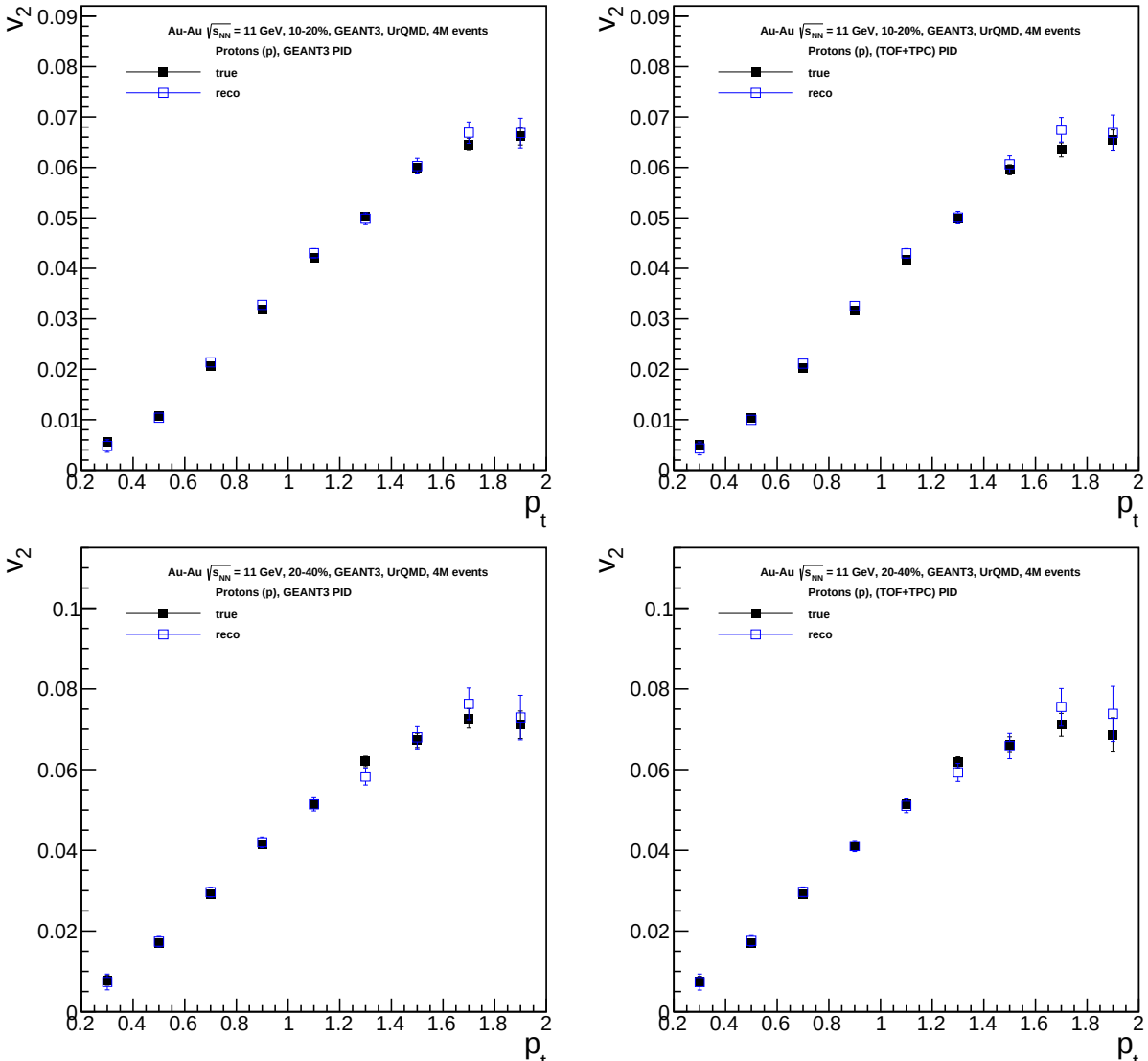

Fig. 19: p_T dependence of v_2 for protons. Upper (lower) rows show v_2 for centrality 10-20% (20-40%). Left (right) columns show ideal (realistic) PID. "true" ("reco") denotes the result obtained with generated from GEANT(reconstructed) values.

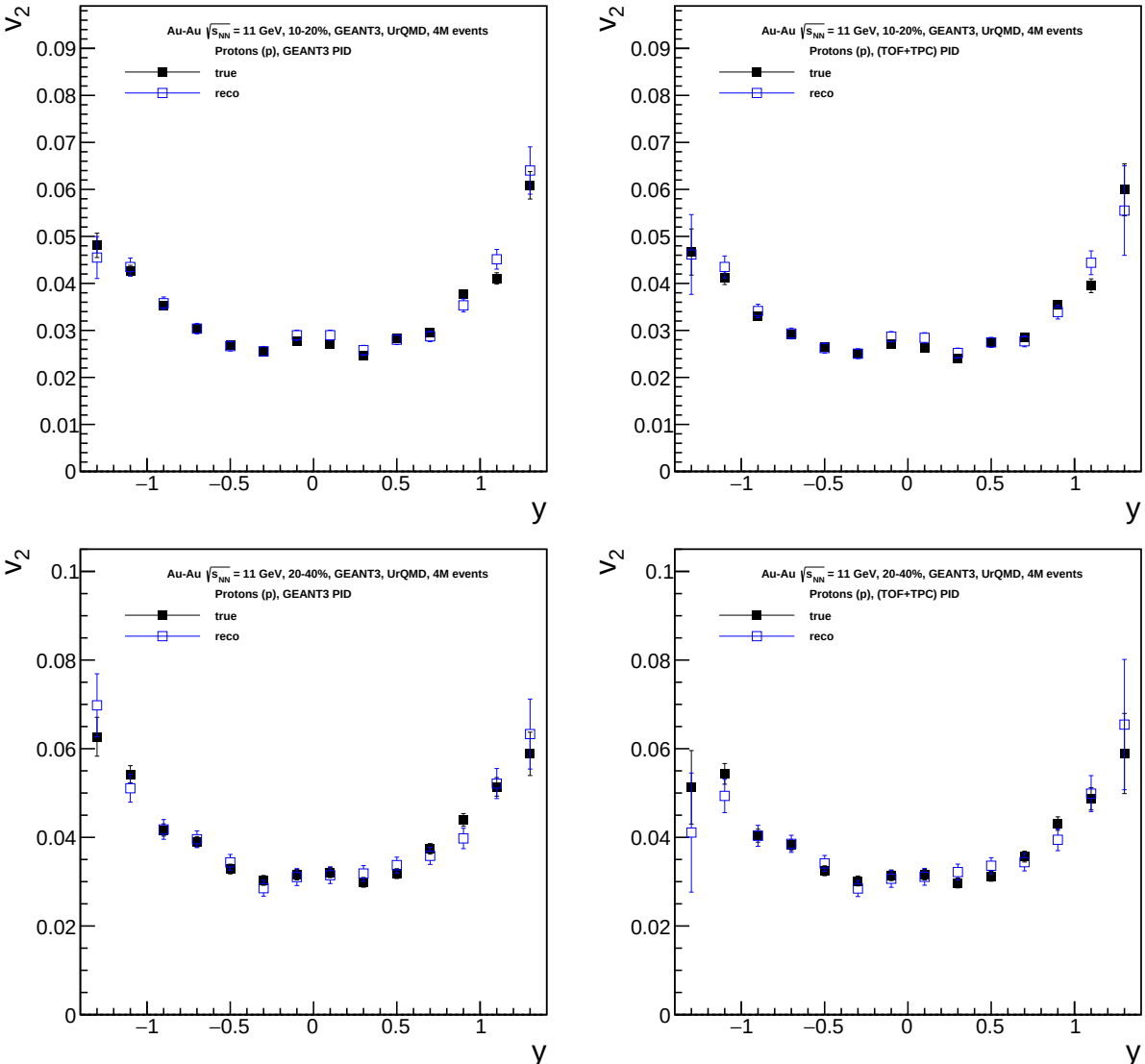

Fig. 20: y dependence of v_2 for protons. Upper (lower) rows show v_2 for centrality 10-20% (20-40%). Left (right) columns show ideal (realistic) PID. "true" ("reco") denotes the result obtained with generated from GEANT(reconstructed) values.

3.2.2.2 ***Kaons***

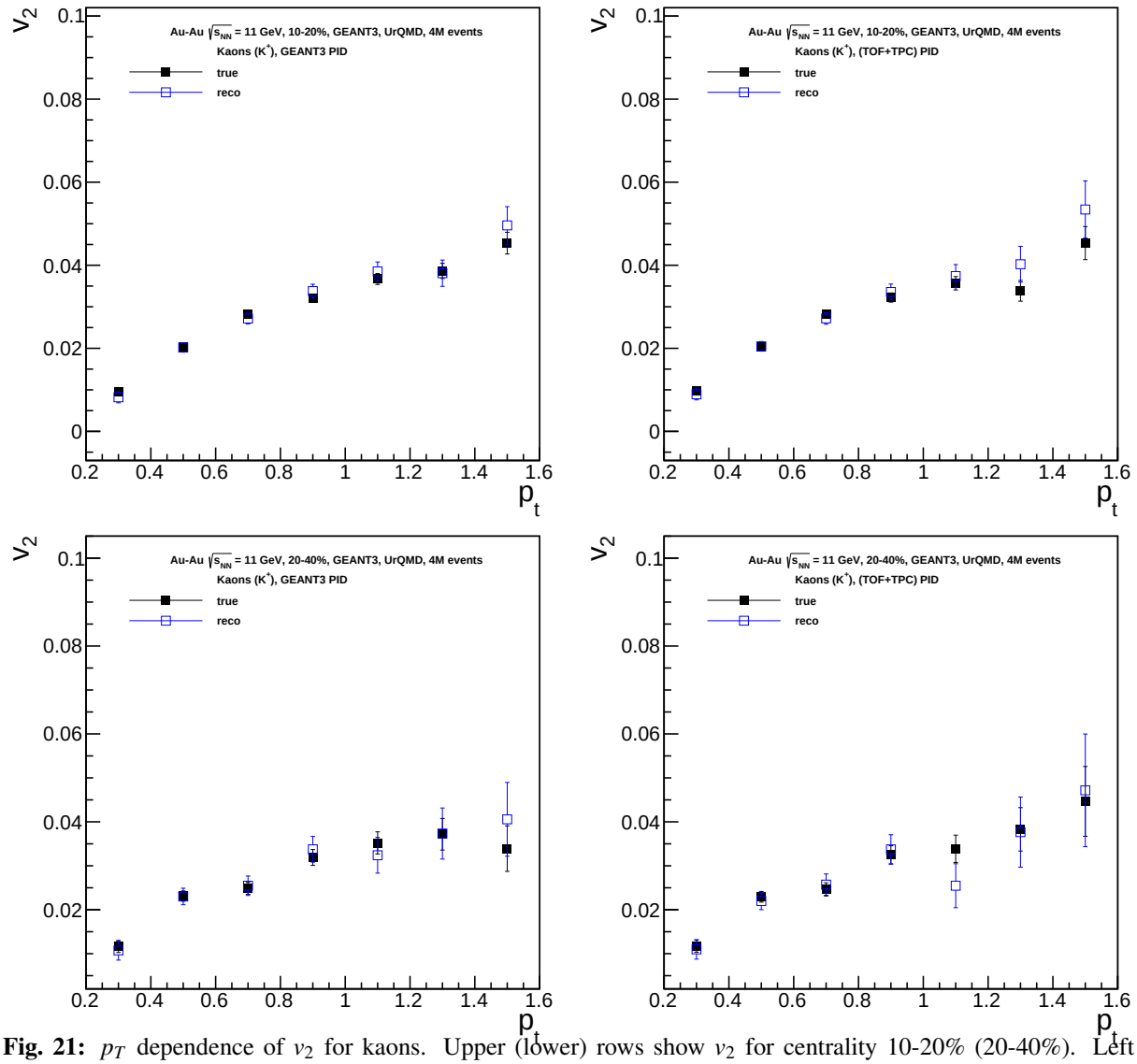

Fig. 21: p_T dependence of v_2 for kaons. Upper (lower) rows show v_2 for centrality 10-20% (20-40%). Left (right) columns show ideal (realistic) PID. ”true” (”reco”) denotes the result obtained with generated from GEANT(reconstructed) values.

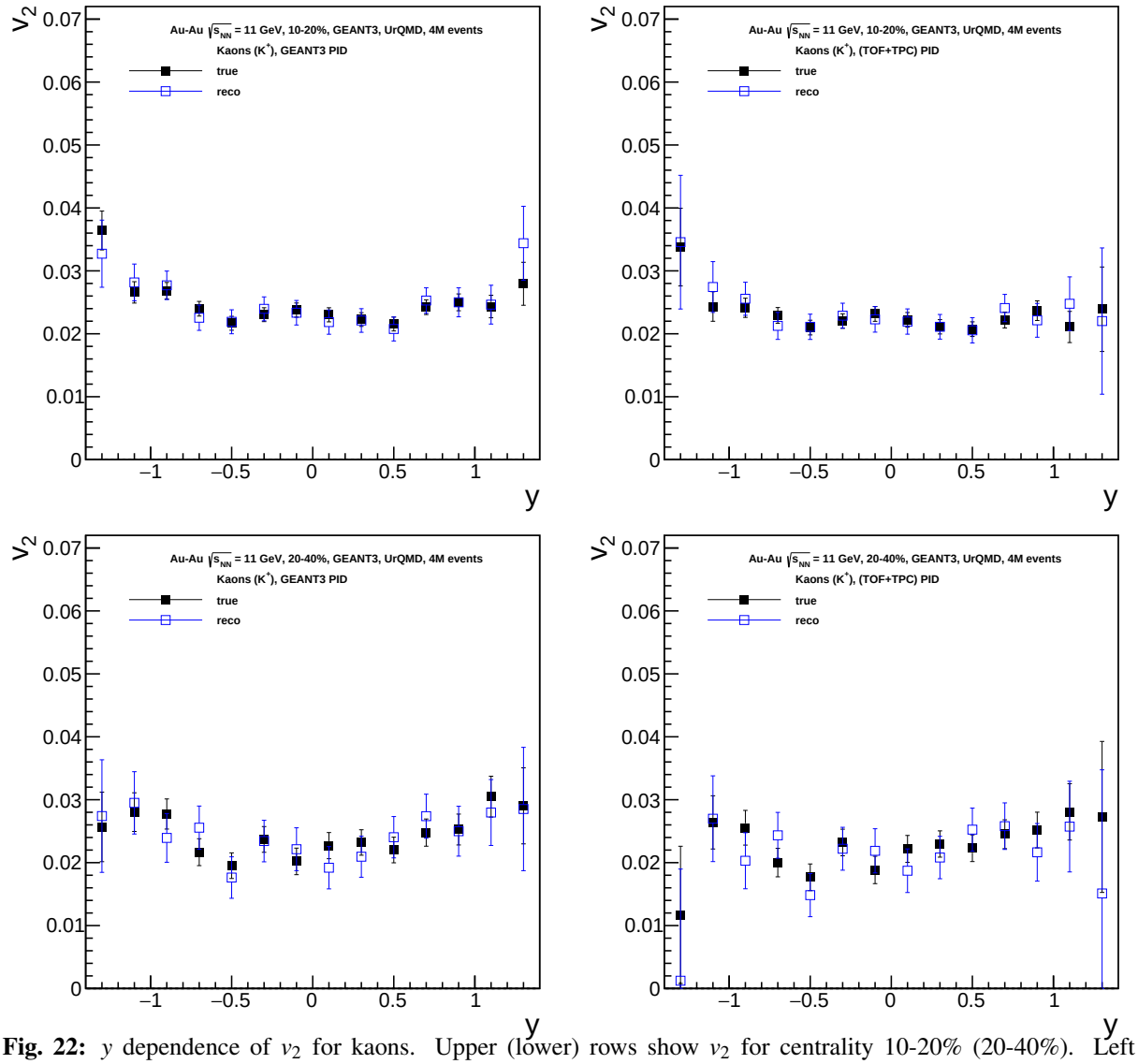

Fig. 22: y dependence of v_2 for kaons. Upper (lower) rows show v_2 for centrality 10-20% (20-40%). Left (right) columns show ideal (realistic) PID. ”true” (”reco”) denotes the result obtained with generated from GEANT(reconstructed) values.

3.2.2.3 ***Pions***

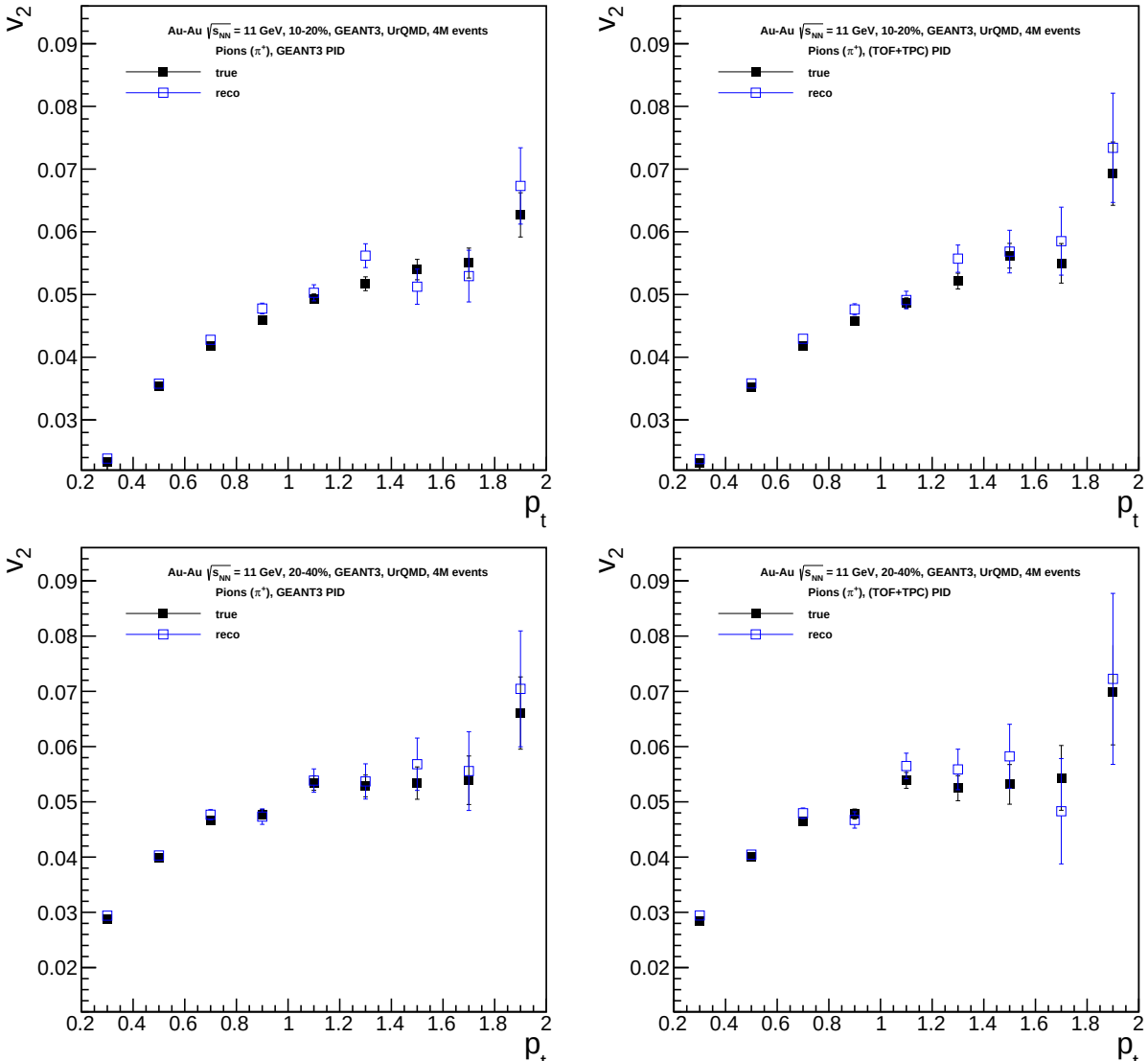

Fig. 23: p_T dependence of v_2 for pions. Upper (lower) rows show v_2 for centrality 10-20% (20-40%). Left (right) columns show ideal (realistic) PID. "true" ("reco") denotes the result obtained with generated from GEANT(reconstructed) values.

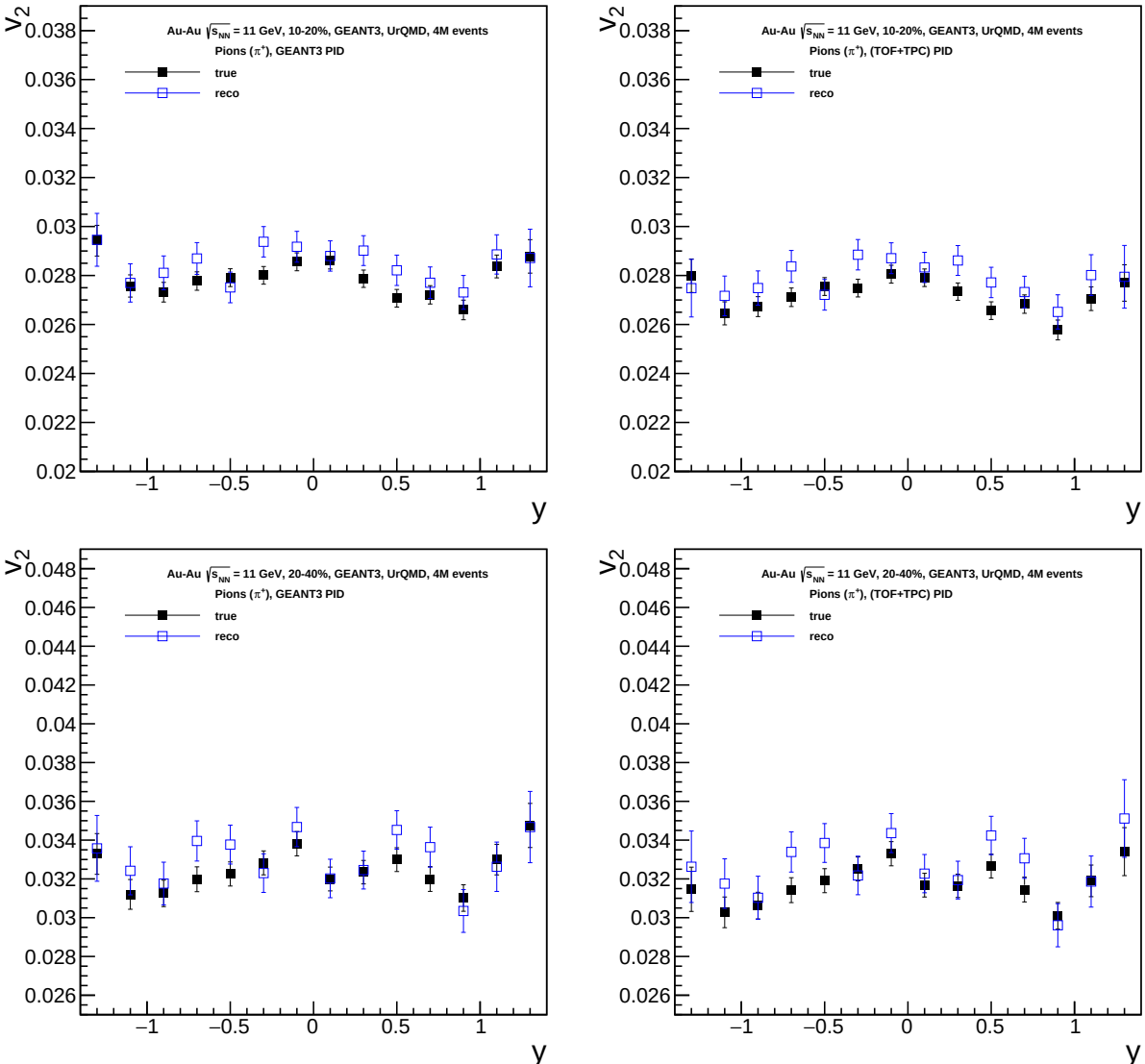

Fig. 24: y dependence of v_2 for pions. Upper (lower) rows show v_2 for centrality 10-20% (20-40%). Left (right) columns show ideal (realistic) PID. "true" ("reco") denotes the result obtained with generated from GEANT(reconstructed) values.

3.3 Compare model prediction and experimental data

In this section, predictions of the models that was used will be compared with the experimental data from the STAR experiment [14, 13, 15] using developed DataReader framework [16]. Simulated data that was used for the comparison:

- UrQMD, $Au+Au$, $\sqrt{s_{NN}} = 7.7$ GeV ($1M$ events), 11.5 GeV ($1M$ events),
- LA-QGSM, $Au+Au$, $\sqrt{s_{NN}} = 7$ GeV ($100k$ events), 11 GeV ($100k$ events).

3.3.1 Event selection

There are 3 centrality regions being used in the further comparison: 0-10%, 10-40% and 40-80% which correspond to $0 < b < 5$ fm, $5 < b < 9$ fm and $9 < b < 15$ fm (see Fig. 25).

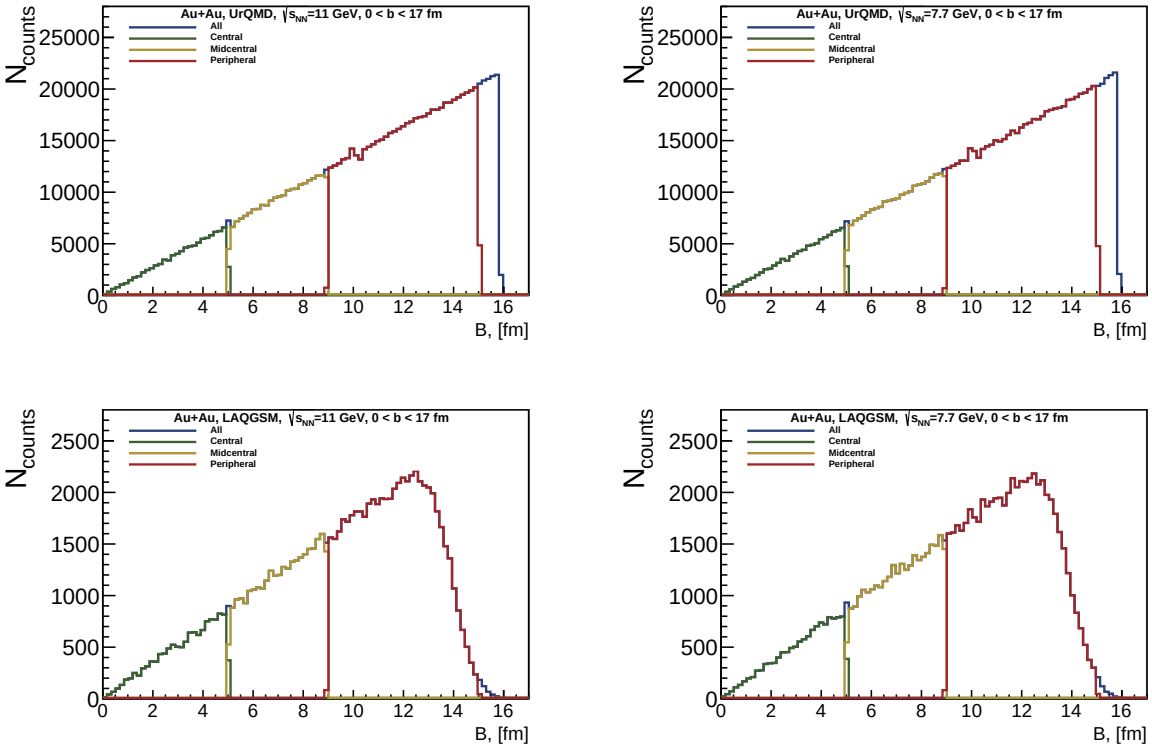

Fig. 25: Event selection based on the impact parameter b for UrQMD (left column) and LA-QGSM (right column) models for $\sqrt{s_{NN}} = 7$ GeV (upper row) and 11 GeV (lower row). Central, midcentral and peripheral regions are shown with different color.

3.3.2 Track selection

Tracks kinematic parameters were selected accordingly to the ones in TPC detector in STAR(see Fig. 26,27):

- PID: protons and pions were selected via PDG codes,
- $0.2 < p_T < 2$ GeV/c,
- $|\eta| < 1$.

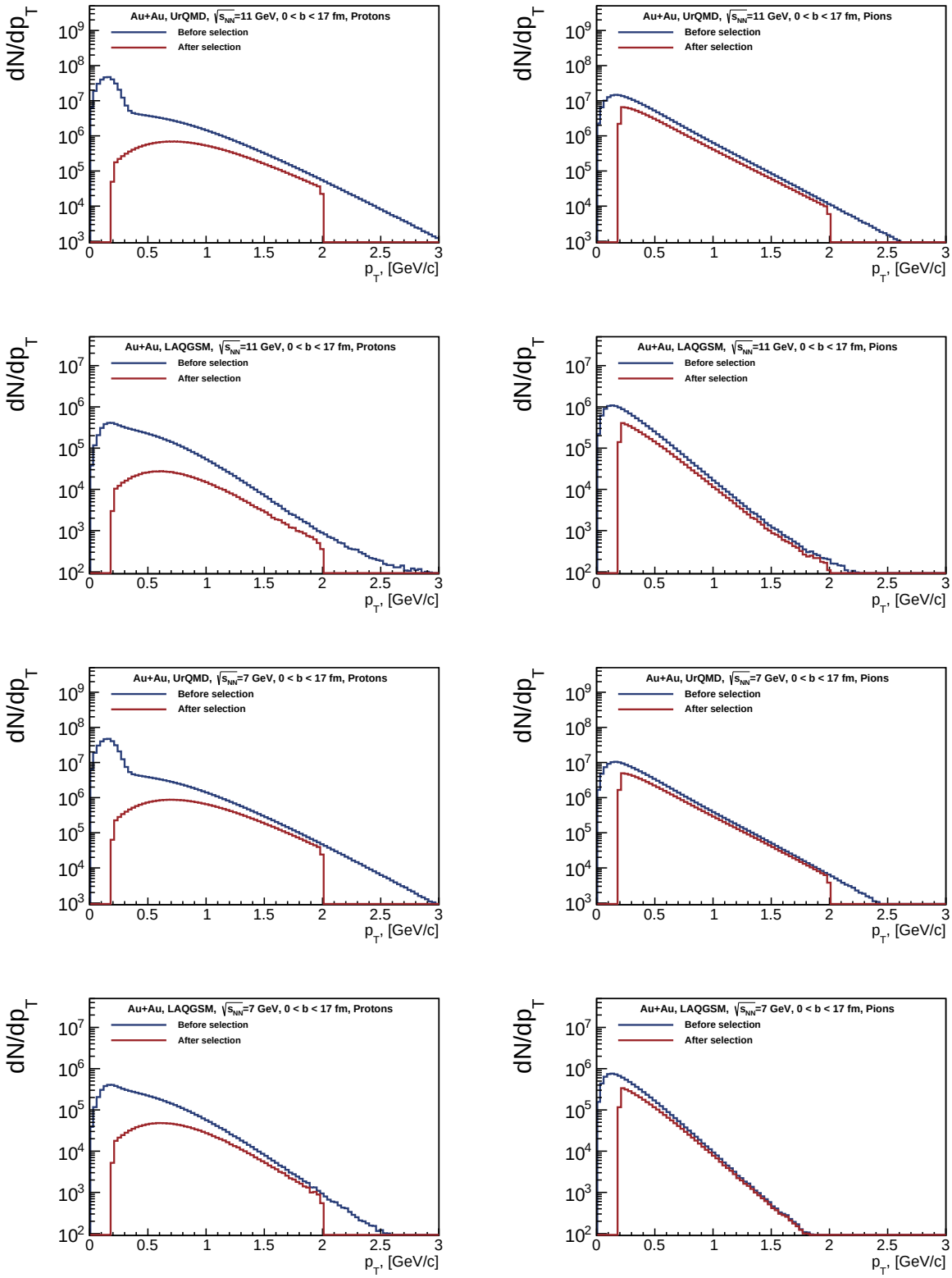

Fig. 26: p_T spectra before and after track selection for protons and pions.

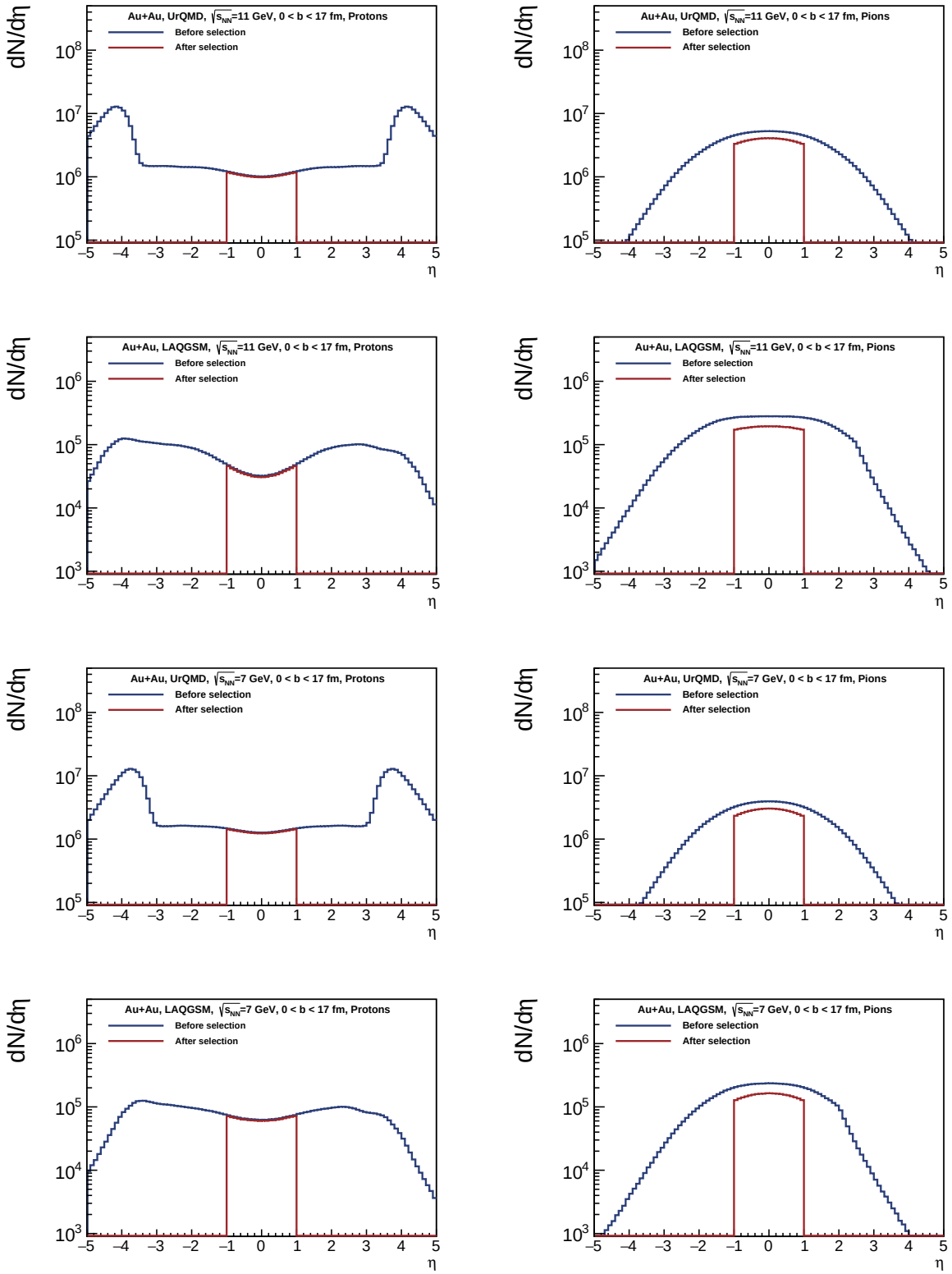

Fig. 27: η spectra before and after track selection for protons and pions.

3.3.3 Directed flow

3.3.3.1 Central collisions

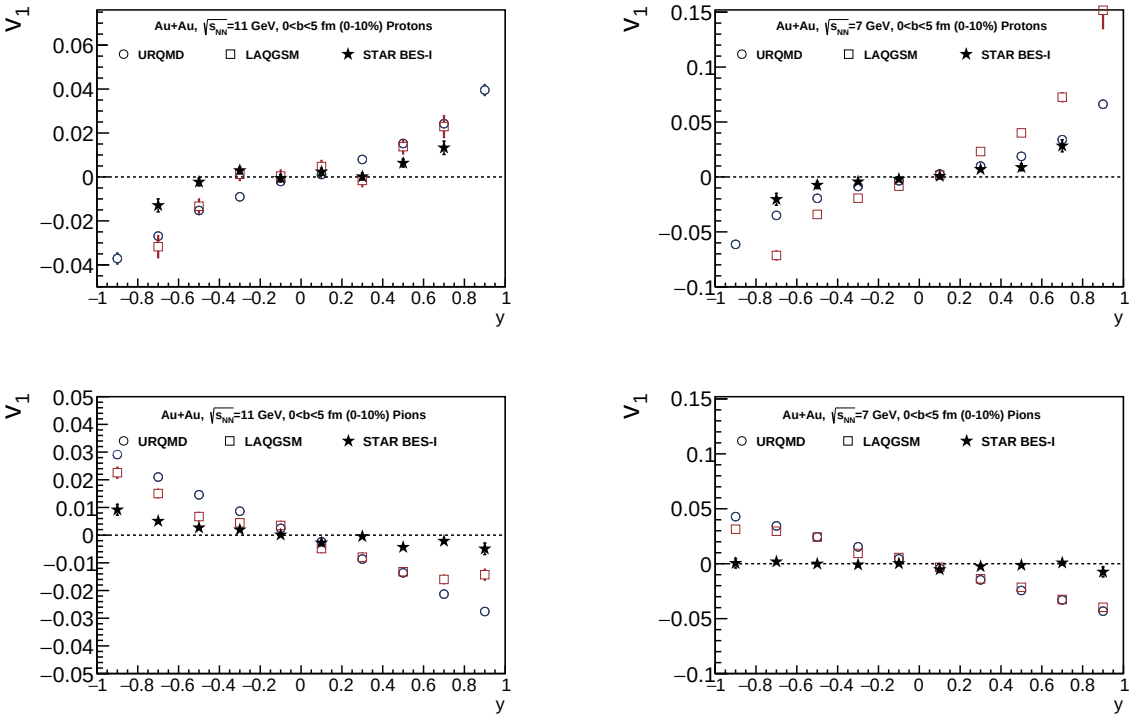

Fig. 28: Directed flow of protons (upper row) and pions (lower row) as a function of rapidity for $\sqrt{s_{NN}} = 11$ GeV (left column) and 7 GeV (right column).

3.3.3.2 Midcentral collisions

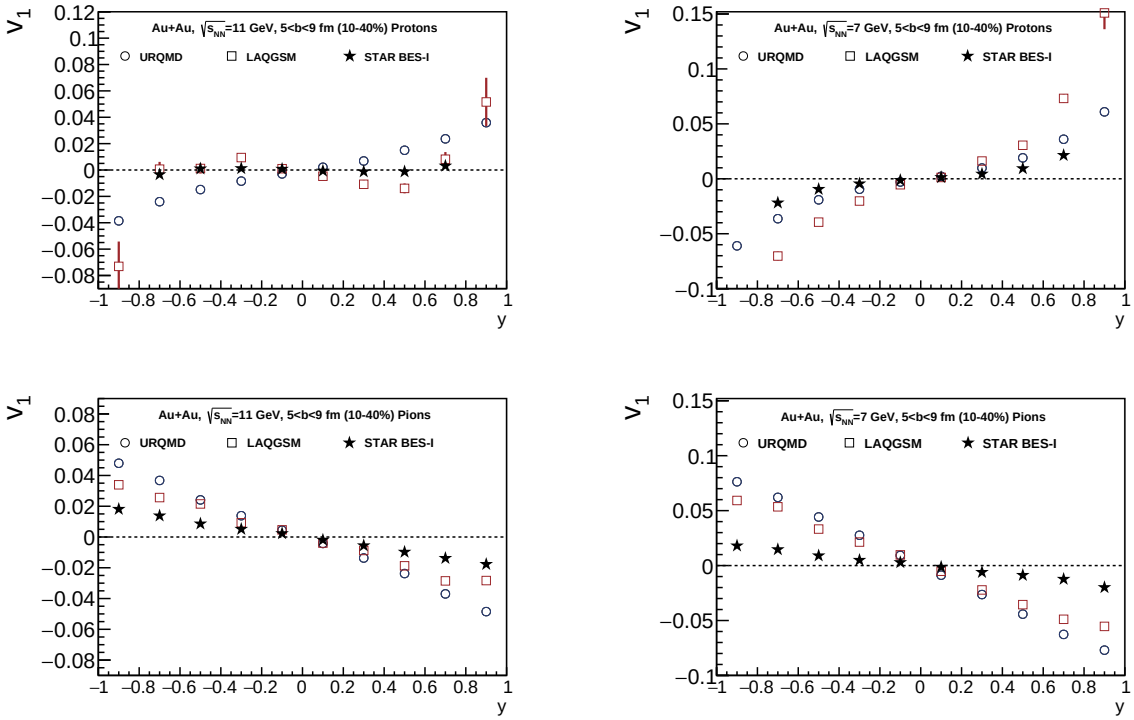

Fig. 29: Directed flow of protons (upper row) and pions (lower row) as a function of rapidity for $\sqrt{s_{NN}} = 11$ GeV (left column) and 7 GeV (right column).

3.3.3.3 ***Peripheral collisions***

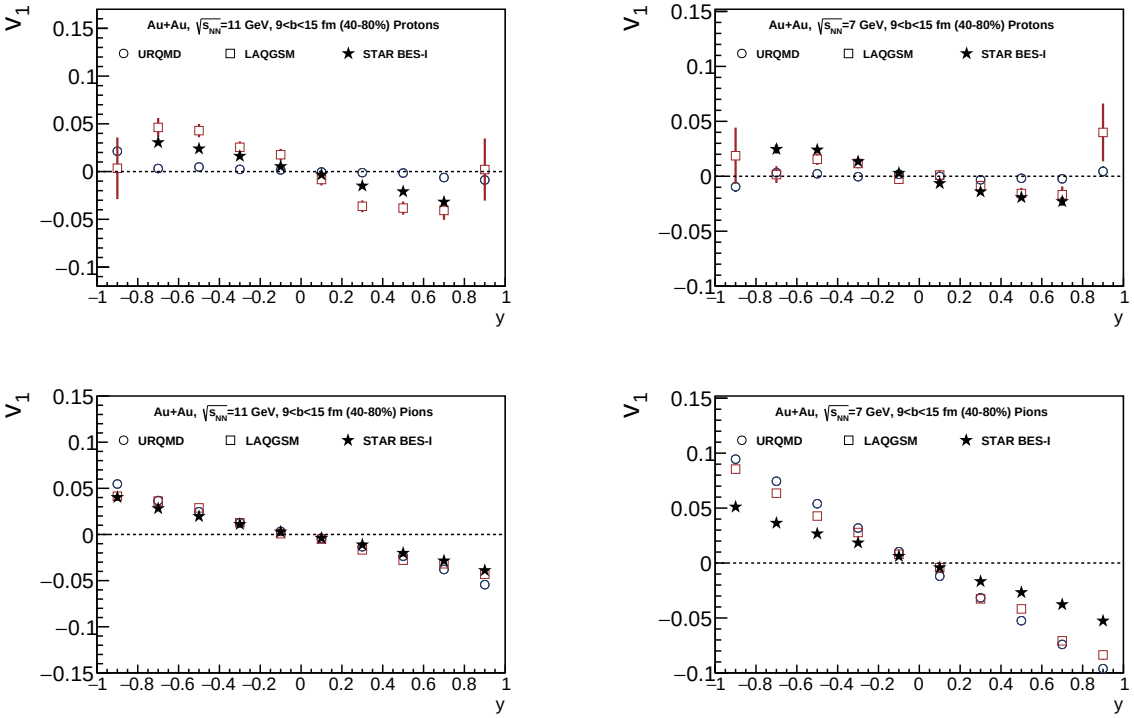

Fig. 30: Directed flow of protons (upper row) and pions (lower row) as a function of rapidity for $\sqrt{s_{NN}} = 11$ GeV (left column) and 7 GeV (right column).

3.3.4 Elliptic flow

3.3.4.1 Central collisions

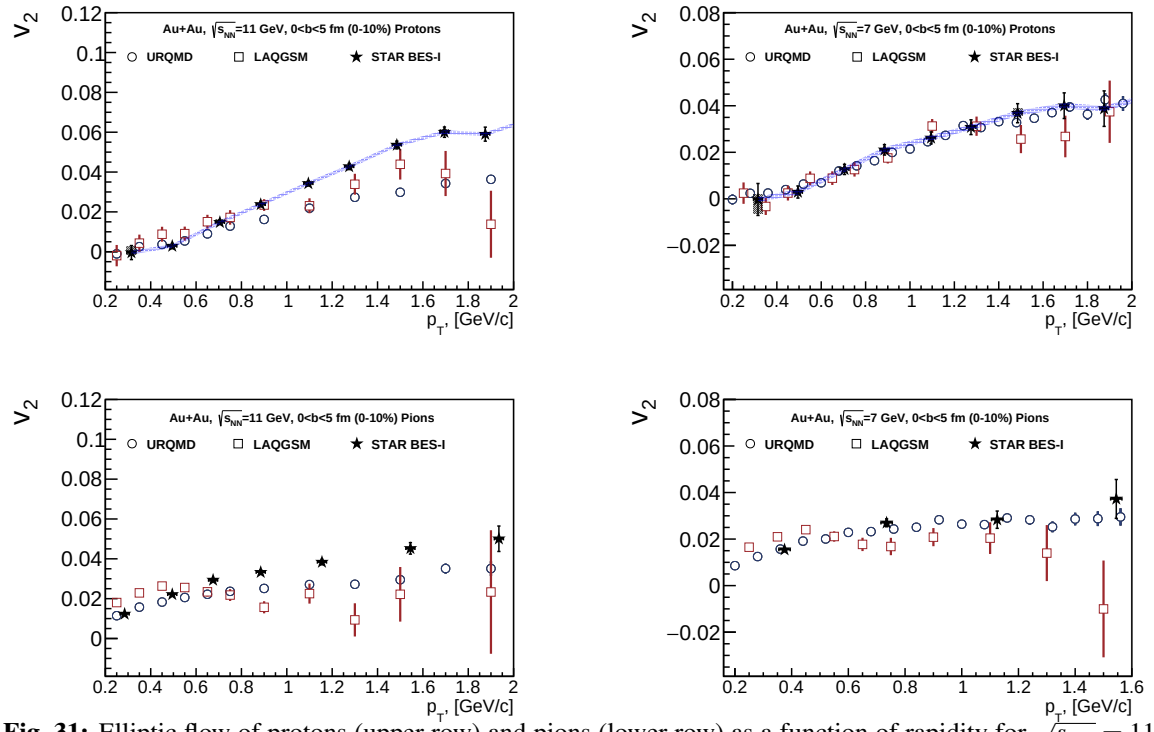

Fig. 31: Elliptic flow of protons (upper row) and pions (lower row) as a function of rapidity for $\sqrt{s_{NN}} = 11$ GeV (left column) and 7 GeV (right column).

3.3.4.2 ***Midcentral collisions***

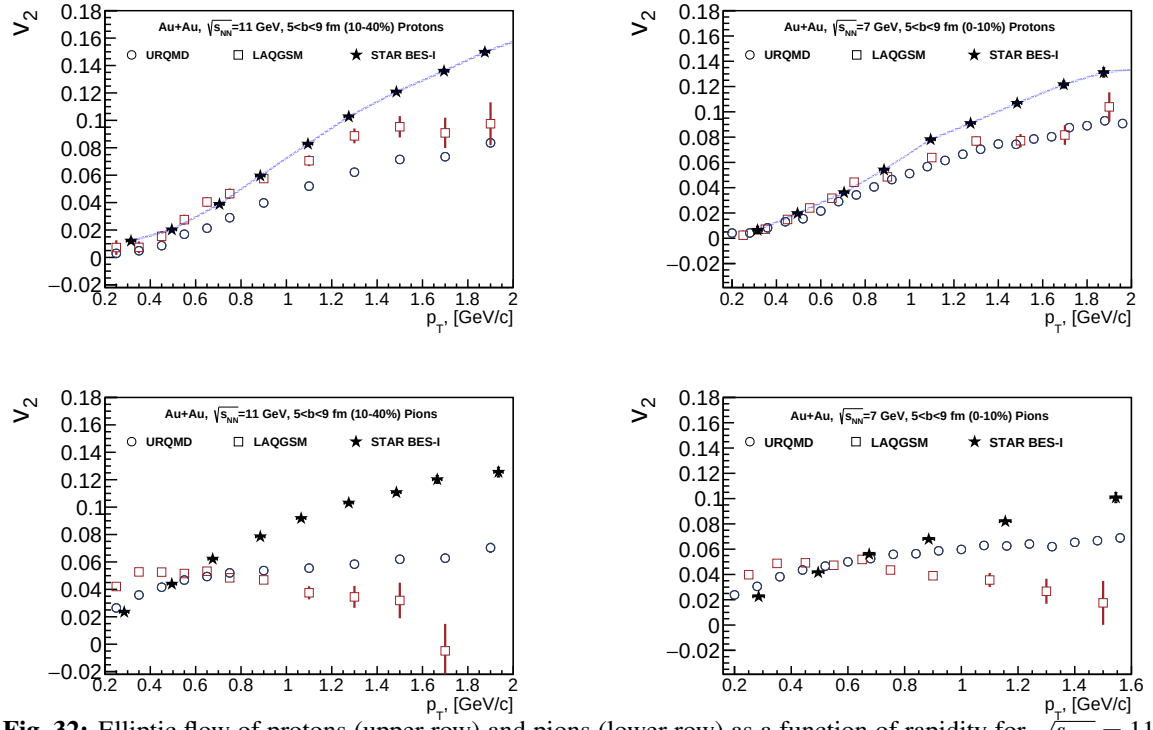

Fig. 32: Elliptic flow of protons (upper row) and pions (lower row) as a function of rapidity for $\sqrt{s_{NN}} = 11$ GeV (left column) and 7 GeV (right column).

3.3.4.3 ***Peripheral collisions***

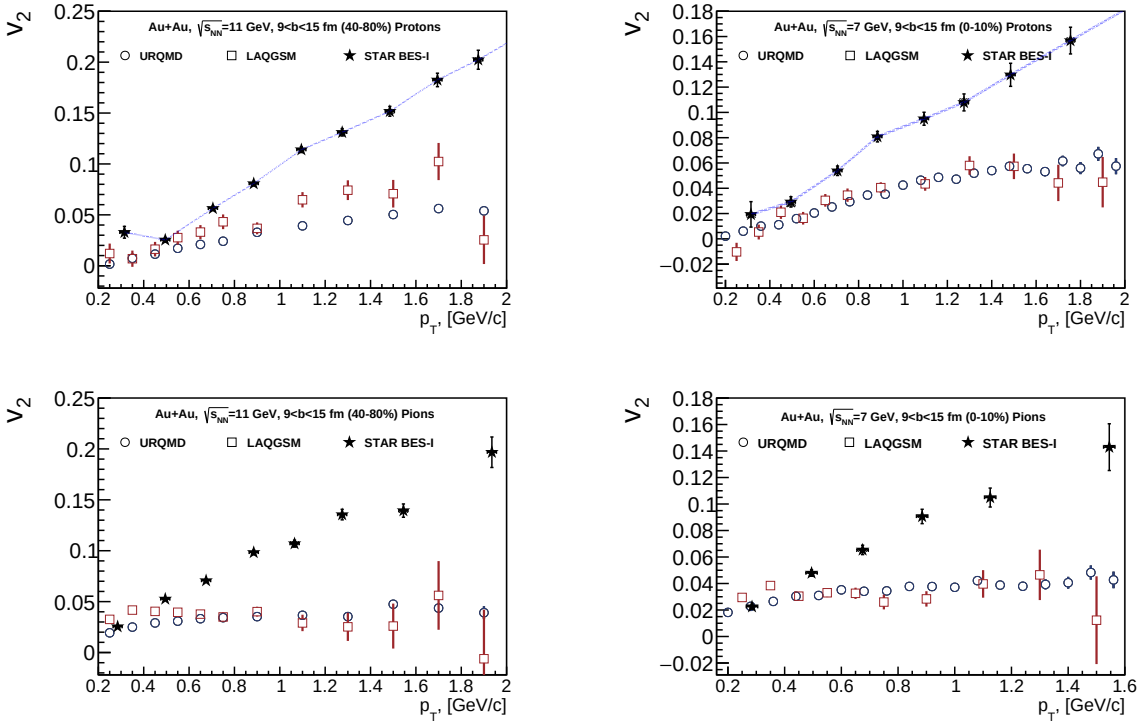

Fig. 33: Elliptic flow of protons (upper row) and pions (lower row) as a function of rapidity for $\sqrt{s_{NN}} = 11$ GeV (left column) and 7 GeV (right column).

4 Summary

Track multiplicity of the emitted charged particles in TPC can be used for centrality determination with resolution 5-10% in a wide centrality range 10-80%. Event plane orientation can be estimated using energy deposition in FHCal with high resolution factor. Directed and elliptic flow were extracted in simulations using event plane method. Results for the reconstructed (reco) and generated (true) values are in good agreement for both particle identification procedures: PDG codes from GEANT and calculated probability from TPC+TOF detectors.

As it is shown on the Fig. 28-33, UrQMD and LA-QGSM predictions for v_1 and v_2 are in good agreement with the STAR data for $\sqrt{s_{NN}} = 7.7$ GeV protons only. Thorough comparison of all available models is in progress.

Acknowledgments

I would like to thank V. I. Kolesnikov for inviting me in the Summer Student Program organized by the JINR University Center. I want to thank my supervisor and scientific advisors: I. V. Selyuzhenkov and A. V. Taranenko for provided guidance. I want to express my gratitude to the University Center of JINR for giving me the opportunity to participate in the Summer Student Program and the management of Veksler and Baldin Laboratory of High Energy Physics for providing a financial support.

References

[1] T. Czopowicz [NA61/SHINE Collaboration], Prog. Theor. Phys. Suppl. **193**, 29 (2012) [arXiv:1201.5829 [hep-ex]].

[2] A. M. Poskanzer and S. A. Voloshin, Phys. Rev. C **58**, 1671 (1998) [nucl-ex/9805001].

[3] M. Golubeva *et al.*, J. Phys. Conf. Ser. **798**, no. 1, 012074 (2017). doi:10.1088/1742-6596/798/1/012074

[4] Technical Design Report for the MPD Experiment: FHCal, http://mpd.jinr.ru/wp-content/uploads/2017/08/MPD_TDR_FHCal_v9_1.pdf

[5] S.A.Bass et al., Prog.Part.Nucl.Phys. 41 (1998) 225

[6] M.Bleicher et al., J.Phys. G25 (1999) 1859

[7] The MultiPurpose Detector (MPD) Concepual Design Report, http://mpd.jinr.ru/wp-content/uploads/2016/04/MPD_CDR_en.pdf

[8] Git link for MPDROOT framework: https://git.jinr.ru/nica/mpdroot/tree/dev

[9] Git link for MPD flow framework: https://git.jinr.ru/nica/mpdroot/tree/dev/macro/physical_analysis/Flow

[10] Git link for MpdPid framework: https://git.jinr.ru/nica/mpdroot/tree/dev/mpdpid

[11] I. A. Svintsov, P. E. Parfenov, I. V. Selyuzhenkov and A. V. Taranenko, J. Phys. Conf. Ser. **798**, no. 1, 012067 (2017).

[12] P. Parfenov, I. Selyuzhenkov, A. Taranenko and A. Truttse, arXiv:1712.09523 [hep-ex].

[13] L. Adamczyk *et al.* [STAR Collaboration], Phys. Rev. Lett. **112**, no. 16, 162301 (2014) doi:10.1103/PhysRevLett.112.162301(2014), 10.1103/PhysRevLett.112.162301 [arXiv:1401.3043 [nucl-ex]].

[14] L. Adamczyk *et al.* [STAR Collaboration], Phys. Rev. C **93**, no. 1, 014907 (2016) doi:10.1103/PhysRevC.93.014907 [arXiv:1509.08397 [nucl-ex]].

[15] L. Adamczyk *et al.* [STAR Collaboration], Phys. Rev. C **88**, 014902 (2013) doi:10.1103/PhysRevC.88.014902 [arXiv:1301.2348 [nucl-ex]].

[16] Git link for DataReader framework: https://github.com/PeterParfenov/DataReader